PARP1 promotes nucleotide excision repair through DDB2 stabilization and recruitment of ALC1

Alex Pines,[1] Mischa G. Vrouwe,[1] Jurgen A. Marteijn,[3] Dimitris Typas,[1] Martijn S. Luijsterburg,[1,6] Medine Cansoy,[1] Paul Hensbergen,[2] André Deelder,[2] Anton de Groot,[1] Syota Matsumoto,[4] Kaoru Sugasawa,[4] Nicolas Thoma,[5] Wim Vermeulen,[3] Harry Vrieling,[1] and Leon Mullenders[1]

[1]Department of Toxicogenetics and [2]Biomolecular Mass Spectrometry Unit, Department of Parasitology, Leiden University Medical Center, 2300 RC Leiden, Netherlands
[3]Department of Genetics, Erasmus MC, 3015 GE Rotterdam, Netherlands
[4]Biosignal Research Center, Graduate School of Science, Kobe University, Nada-ku, Kobe 657-8501, Japan
[5]Friedrich Miescher Institute for Biomedical Research, CH-4058 Basel, Switzerland
[6]Department of Cell and Molecular Biology, Karolinska Institutet, S-17177 Stockholm, Sweden

The WD40-repeat protein DDB2 is essential for efficient recognition and subsequent removal of ultraviolet (UV)-induced DNA lesions by nucleotide excision repair (NER). However, how DDB2 promotes NER in chromatin is poorly understood. Here, we identify poly(ADP-ribose) polymerase 1 (PARP1) as a novel DDB2-associated factor. We demonstrate that DDB2 facilitated poly(ADP-ribosyl)ation of UV-damaged chromatin through the activity of PARP1, resulting in the recruitment of the chromatin-remodeling enzyme ALC1.

Depletion of ALC1 rendered cells sensitive to UV and impaired repair of UV-induced DNA lesions. Additionally, DDB2 itself was targeted by poly(ADP-ribosyl)ation, resulting in increased protein stability and a prolonged chromatin retention time. Our in vitro and in vivo data support a model in which poly(ADP-ribosyl)ation of DDB2 suppresses DDB2 ubiquitylation and outline a molecular mechanism for PARP1-mediated regulation of NER through DDB2 stabilization and recruitment of the chromatin remodeler ALC1.

Introduction

Nucleotide excision repair (NER) is a multistep process that mediates the removal of structurally and chemically diverse DNA lesions including UV light–induced cyclobutane pyrimidine dimers (CPDs) and 6-4 pyrimidine pyrimidone photoproducts (6-4PPs). The importance of NER in protecting organisms against solar UV-induced DNA damage is underscored by the hereditary disease xeroderma pigmentosum (XP), which is clinically characterized by hypersensitivity to sunlight and predisposition to skin cancer (Cleaver et al., 2009). XP has been linked to defects in seven proteins (XP-A through XP-G) that, with the exception of XPC and XPE (hereafter named DDB2), function in the core NER reaction. The proteins encoded by the XPC and XPE genes are involved in the global genome NER

subpathway (GG-NER) but are dispensable for transcription-coupled NER (TC-NER; Cleaver et al., 2009).

Reconstitution of the NER reaction with purified proteins has defined the minimal set of proteins required for GG-NER in vitro (Aboussekhra et al., 1995). The initial step of DNA damage recognition depends on the XPC–Rad23 complex and subsequently results in local DNA unwinding and damage verification by the basal transcription factor TFIIH, the single-stranded DNA (ssDNA)–binding complex RPA, and XPA. Dual incision of the damaged DNA strand is carried out by the 5′ and 3′ structure-specific endonucleases XPF-ERCC1 and XPG, respectively, followed by gap filling and DNA ligation (Aboussekhra et al., 1995).

DNA damage recognition by XPC involves the detection of unpaired bases (Min and Pavletich, 2007; Clement et al., 2010), which renders lesion recognition of minor helix-distorting lesions such as CPDs very inefficient (Sugasawa et al., 2001).

In addition to XPC, efficient repair of CPDs therefore requires the heterodimeric UV-DDB protein complex consisting of the DDB1 and DDB2 subunits (Fitch et al., 2003; Moser et al., 2005). The crystal structure of UV-DDB bound to a 6-4PP–containing DNA duplex revealed the direct and exclusive binding of DDB2 to the photodimer (Scrima et al., 2008). XP-E cells lacking functional DDB2 are deficient in repair of CPDs but competent in repair of 6-4PPs, albeit at reduced rates (Hwang et al., 1999; Moser et al., 2005). This partial requirement for UV-DDB in GG-NER is reflected in the relative mild sensitivity of XP-E cells to UV-induced cell death (Tang and Chu, 2002). Although UV-DDB deficiency impairs repair of photolesions in vivo, it is dispensable for NER in vitro (Aboussekhra et al., 1995; Mu et al., 1995; Rapić Otrin et al., 1998), suggesting that UV-DDB is important for the repair of DNA lesions in a chromatin context.

The UV-DDB complex interacts with several factors known to modulate chromatin structure such as histone acetyltransferase p300, the STAGA complex (Datta et al., 2001; Martinez et al., 2001; Rapić-Otrin et al., 2002), and the Cullin-RING ubiquitin ligase (CRL4) complex CUL4A–RBX1 (Shiyanov et al., 1999; Groisman et al., 2003). The CRL4–DDB2 complex ubiquitylates DDB2 and XPC in response to UV irradiation, which facilitates efficient recognition of photolesions by XPC (Sugasawa et al., 2005). Moreover, the CRL4 complex also ubiquitylates histones H2A, H3, and H4 (Kapetanaki et al., 2006), of which H3 and H4 ubiquitylation affects nucleosome stability (Wang et al., 2006).

Despite these studies, the molecular mechanisms through which UV-DDB facilitates recognition of DNA damage in chromatin remain poorly understood. Here we purified DDB2 and associated factors from human cells and identified poly(ADP-ribose) (PAR) polymerase 1 (PARP1) as a novel component of the UV-DDB complex. We provide evidence for a central role of DDB2-associated PARP1 in mediating PAR synthesis and recruitment of the SWI/SNF chromatin remodeler ALC1 to UV-damaged DNA. Moreover, we show that poly(ADP-ribosyl)ation of DDB2 itself regulates the stability as well as the chromatin retention time of DDB2. Interfering with either PARP1 or ALC1 function impairs CPD repair and renders cells highly sensitive to UV irradiation. Together, these findings outline a novel molecular mechanism for the DDB2-mediated and PARP1-executed regulation of NER.

Results

PARP1 is a component of the UV-DDB complex

To identify novel factors involved in the DNA damage recognition step of GG-NER, we isolated DDB2-associated protein complexes by chromatin immunoprecipitation (Fig. 1, A and B) and analyzed purified proteins by mass spectrometry (MS). MRC5 cells expressing FLAG-tagged DDB2 were either mock treated or irradiated with 20 J/m^2 UV-C light and incubated for 5 min before chromatin isolation and immunoprecipitation using FLAG antibody. MS analysis identified several proteins known to interact with DDB2, including DDB1, CUL4A, CUL4B, and

components of the COP9 signalosome (Table S1), showing that native DDB2 is indeed isolated from cells using this approach. Interestingly, multiple DDB2 peptides were identified by MS with protein masses exceeding 50 kD in UV-irradiated cells but not in mock-treated cells (Fig. 1 A), suggesting the presence of UV-specific posttranslational modifications of DDB2. In addition to these known factors, we also identified PARP1 as a novel DDB2-associated factor. We confirmed the interaction between endogenous DDB2 and endogenous PARP1 by reciprocal immunoprecipitation experiments (Fig. 1 C) using chromatin prepared from UV-irradiated or mock-treated normal human fibroblasts (NHFs). These results show that UV irradiation stimulates the interaction between the UV-DDB complex and PARP1 on chromatin. Moreover, an interaction between recombinant UV-DDB and recombinant PARP1 could indeed be detected in vitro, supporting a direct interaction between these factors (Fig S1, A and B). To test which subunit of the UV-DDB complex interacts with PARP1, we purified GFP-DDB1 or GFP-DDB2 under denaturing conditions from cells. The results revealed that both DDB1 and DDB2 interact with PARP1 (Fig. 1 D). Consistent with this notion, we found that GFP-DDB2^{D307Y}, which is unable to form a complex with DDB1 (Luijsterburg et al., 2012), also binds PARP1, indicating that DDB2–PARP1 interaction does not require DDB1. To corroborate these findings, we isolated GFP-DDB1 or GFP-DDB2 from polyacrylamide gels and found both extracted proteins to interact with PARP1 in vitro (Fig. S1 C). Finally, far-Western blotting also revealed that both DDB1 and DDB2 avidly bind to PARP1 (Fig. S1 B). Together, our findings reveal a novel and direct interaction between the UV-DDB complex and PARP1, which prompted us to assess the involvement of PARP1 in modifying DDB2 and regulating NER.

PAR chains are synthesized at UV-induced DNA lesions

We first assessed whether PAR chains are synthesized in chromatin containing UV-induced DNA lesions. To this end, we locally irradiated G0/G1 synchronized telomerase-immortalized human fibroblasts with UV-C light (254 nm) through a polycarbonate mask (Moné et al., 2001). Staining with specific antibodies revealed the presence of PAR chains at sites of DNA damage marked by the recruitment of the p89 subunit of TFIIH or replication factor PCNA known to be involved in NER (Fig. 2, A and B). Moreover, PAR staining in Ki67-negative cells confirmed that PAR synthesis occurred at DNA lesions in nonproliferating cells, underlining the replication-independent nature of these events (Fig. 2 C). Finally, chemical inhibition of PARP1 impaired the formation of PAR chains at damaged sites (Fig. 2 D), indicating that the activity of PARP1 is responsible for PAR synthesis at sites of local UV damage.

PAR glycohydrolase (PARG) and DNA synthesis inhibition modulate UV-dependent PARylation

We noted during our experiments that the synthesis of PAR chains at DNA lesions was only detectable in a subset of cells (Fig. 2, A and B). To gain insight into this phenomenon, we locally UV irradiated human fibroblasts with different doses
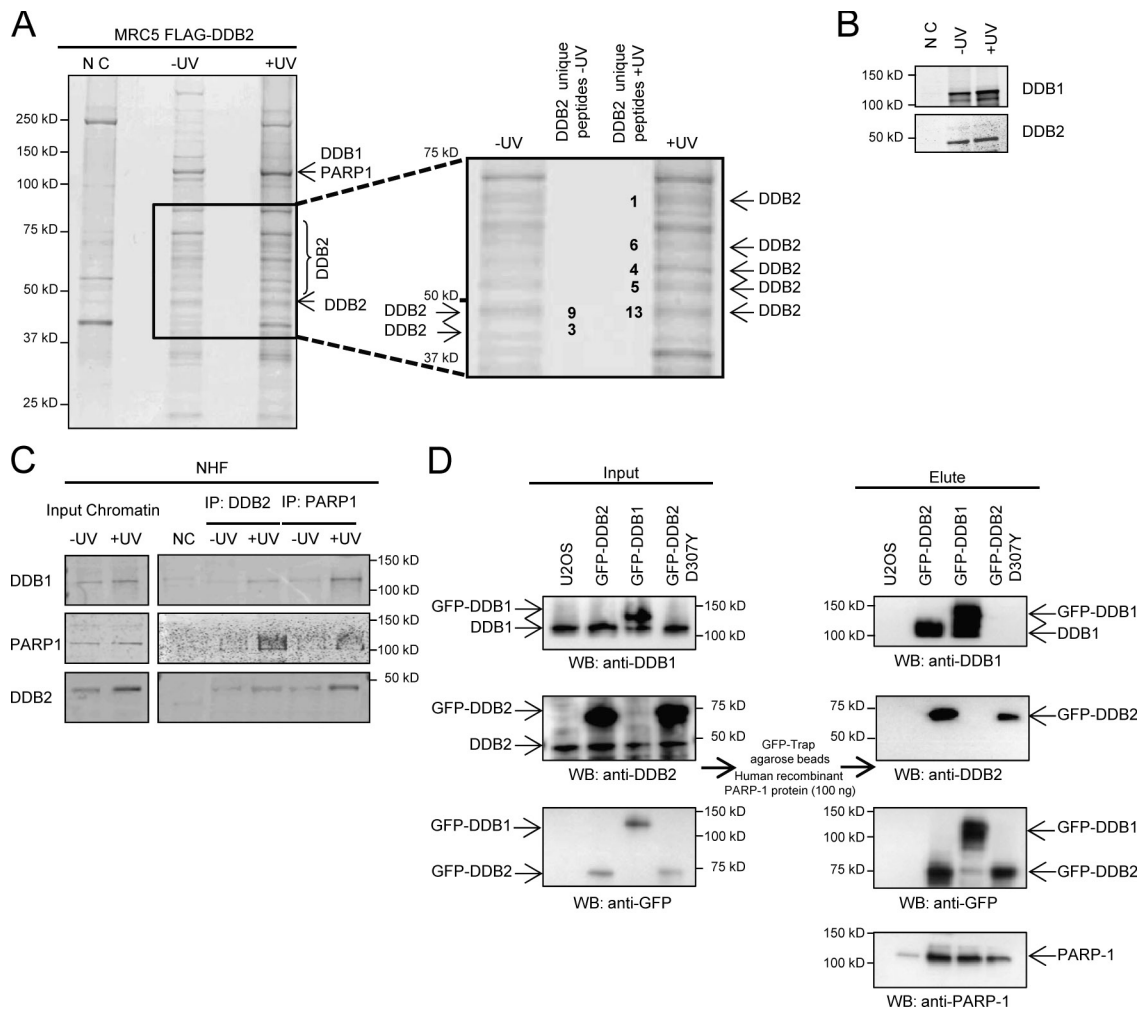
Figure 1. **PARP1 is a novel DDB2-associated factor.** (A) SDS-PAGE electrophoresis and Coomassie staining of FLAG-DDB2 immunoprecipitates obtained from FLAG-DDB2–expressing MRC5 cells mock treated or irradiated with 20 J/m^2 UV-C. Negative control (NC) indicates the eluate obtained from agarose beads incubated with MRC5 FLAG-DDB2 chromatin. The arrows in the zoom-in window indicate the position of the gel where DDB2 and the respective unique peptides were detected by MS (a unique peptide is defined as a peptide, irrespective of its length, that exists only in one protein of a proteome of interest). (B) Western blot of FLAG-DDB2 immunoprecipitates. Cells were mock treated or irradiated with 20 J/m^2 UV-C and immunoblotted with DDB1- and DDB2-specific antibodies. Negative control indicates the eluate obtained from agarose beads incubated with chromatin from MRC5 FLAG-DDB2 cells. (C) Western blot of DDB2 and PARP1 immunoprecipitates (IP) from NHF cells mock treated or irradiated with 20 J/m^2 UV-C, followed by 5-min incubation, and immunoblotted against DDB1, DDB2, or PARP1. (D) GFP-DDB2–PARP-1 binding assay. U2OS cells transfected with the indicated GFP constructs were lysed in denaturing buffer and subjected to immunoprecipitation with GFP-TRAP beads and then incubated with 100 ng purified recombinant PARP-1. The beads were then processed for immunoblotting. WB, Western blot.

(30 or 100 J/m^2) and subsequently monitored the formation of PAR chains 30 min after irradiation (Fig. 2 E). The percentage of cells with PAR chains at sites of local damage significantly increased between 30 and 100 J/m^2 but did not exceed 50% of the cells (Fig. 2, E and F). It is known that the transient and highly dynamic nature of PAR chains is caused by the rapid reversal of this modification by the activity of PARG (Slade et al., 2011). To increase the steady-state level of UV-induced PAR chains, we lowered the levels of PARG by siRNAs. Indeed, depletion of PARG resulted in a significantly elevated percentage of cells that displayed PAR chains at DNA lesions, which was roughly 60% at 30 J/m^2 and 75% at 100 J/m^2 (Fig. 2, E and F). These findings show that UV-induced PAR chains are formed in the majority of cells but are rapidly reversed by the activity of PARG. We then hypothesized that ssDNA gaps transiently generated during NER might elicit the synthesis of PAR chains.

In support of this, we found that inhibition of DNA synthesis and ligation by hydroxyurea (HU) and cytosine-β-arabinofuranoside (AraC), known to result in the formation of persistent ssDNA gaps (Overmeer et al., 2011), resulted in robust PAR synthesis in all UV-irradiated cells (Fig. 2, E and F).

DDB2 mediates PARylation during the preincision stage of NER

To evaluate whether UV-induced PAR synthesis was exclusively dependent on the presence of an ssDNA repair intermediate, we examined PARylation in XP-A cells that are unable to perform incision and thus do not accumulate ssDNA (Fig. 3 C; Friedberg, 2001). Indeed, PAR synthesis could not be detected in XP-A cells even after treatment with HU and AraC (Fig. 3, A and B), consistent with a role of dual incision in triggering these events. Strikingly, however, the formation

Figure 2. **PARylation of chromatin at sites of UV lesions.** (A–D) NHF cells were locally UV irradiated (100 J/m²), fixed after the indicated time, and stained with an antibody recognizing PAR, TFIIH, PCNA, or Ki67. PAR colocalizes with the damage markers TFIIH and PCNA (A and B) including noncycling cells (Ki67-negative staining; C). Treatment with 10 µM of a specific PARPi resulted in a complete loss of PAR signal (D). Arrows indicate local damage sites. (E) NHF cells were transfected with the indicated siRNA or treated with HU/AraC. 48 h after transfection, the cells were locally UV exposed (30 or 100 J/m²), fixed after the indicated time, and stained with an antibody recognizing PAR or TFIIH. Bars, 20 µm. (F) The percentage of colocalization of PAR with TFIIH in NHF cells is plotted for the different siRNA transfections and HU/AraC treatment. The results are from three independent experiments in which about 100 cells per condition were analyzed. Error bars indicate SD. The data shown are from a single representative experiment out of three repeats.
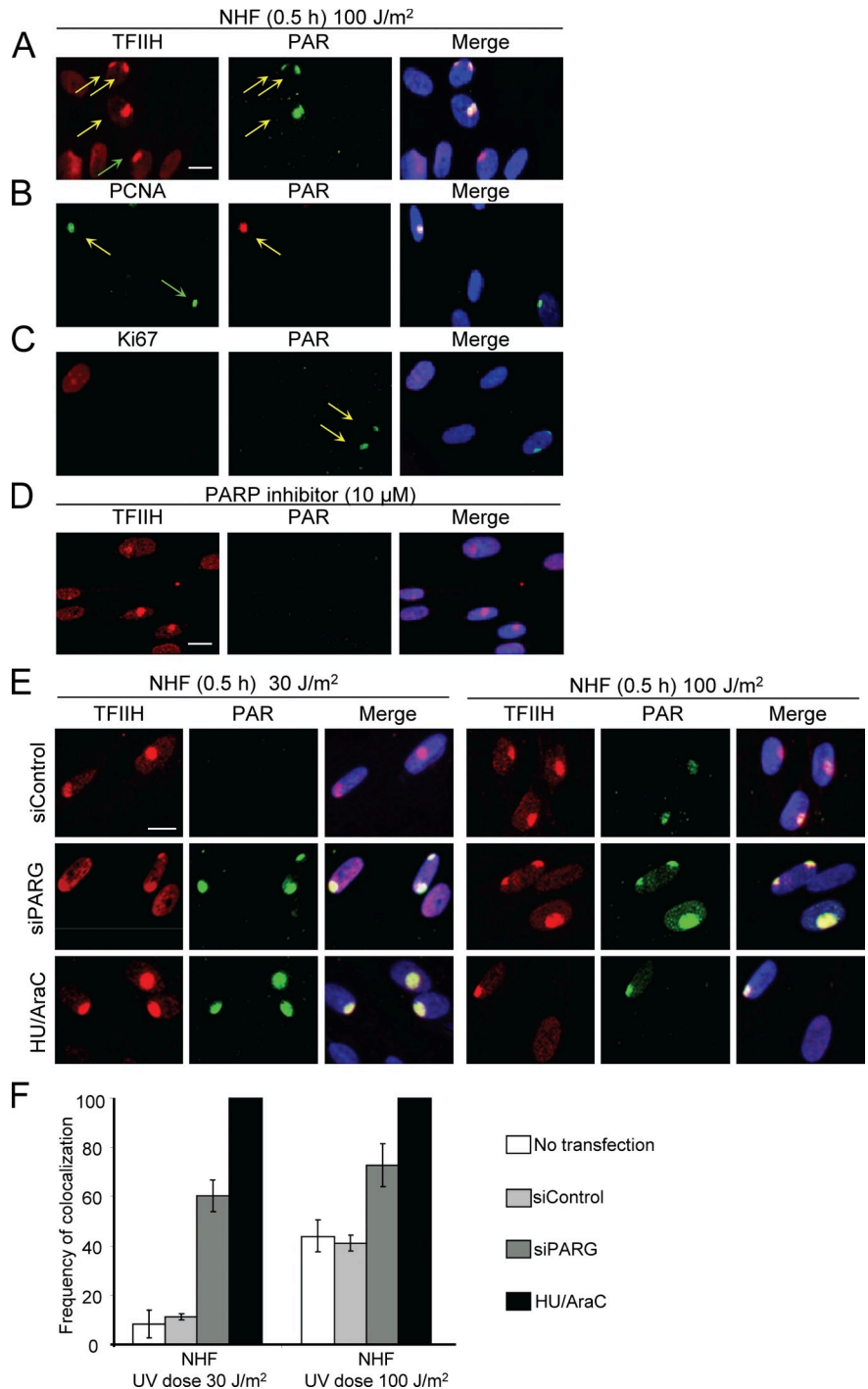
of PAR chains was still detected in XP-A cells upon the depletion of PARG (Fig. 3, A and B), suggesting that PAR chain formation is not solely dependent on the formation of ssDNA. Given our finding that UV-DDB interacts with PARP1, we addressed whether DDB2 contributes to PAR synthesis at sites of DNA damage. At later time points after UV irradiation (30 min after 100 J/m²), when stretches of ssDNA had been generated, we detected a substantial difference in PAR synthesis between normal human cells and DDB2-deficient XP-E cells as only 10% of the XP-E cells displayed clear PARylation at damaged sites when compared with normal cells (Fig. 3, D and E).

However, similar to repair-proficient cells, we found inhibition of PAR turnover by PARG depletion to increase the percentage of PAR-positive cells to about 40%, whereas inhibition of DNA synthesis resulted in PAR synthesis at all locally damaged sites (Fig. 3, D and E). These findings are consistent with the notion that XP-E cells are impaired in dual incision because of deficient repair of CPDs and underscore the role of ssDNA formation in UV-induced PAR synthesis. During the time period of 30 min after UV irradiation, a substantial part of repair represents removal of 6-4PPs being repaired much more rapidly than CPDs. XPE cells display efficient repair of
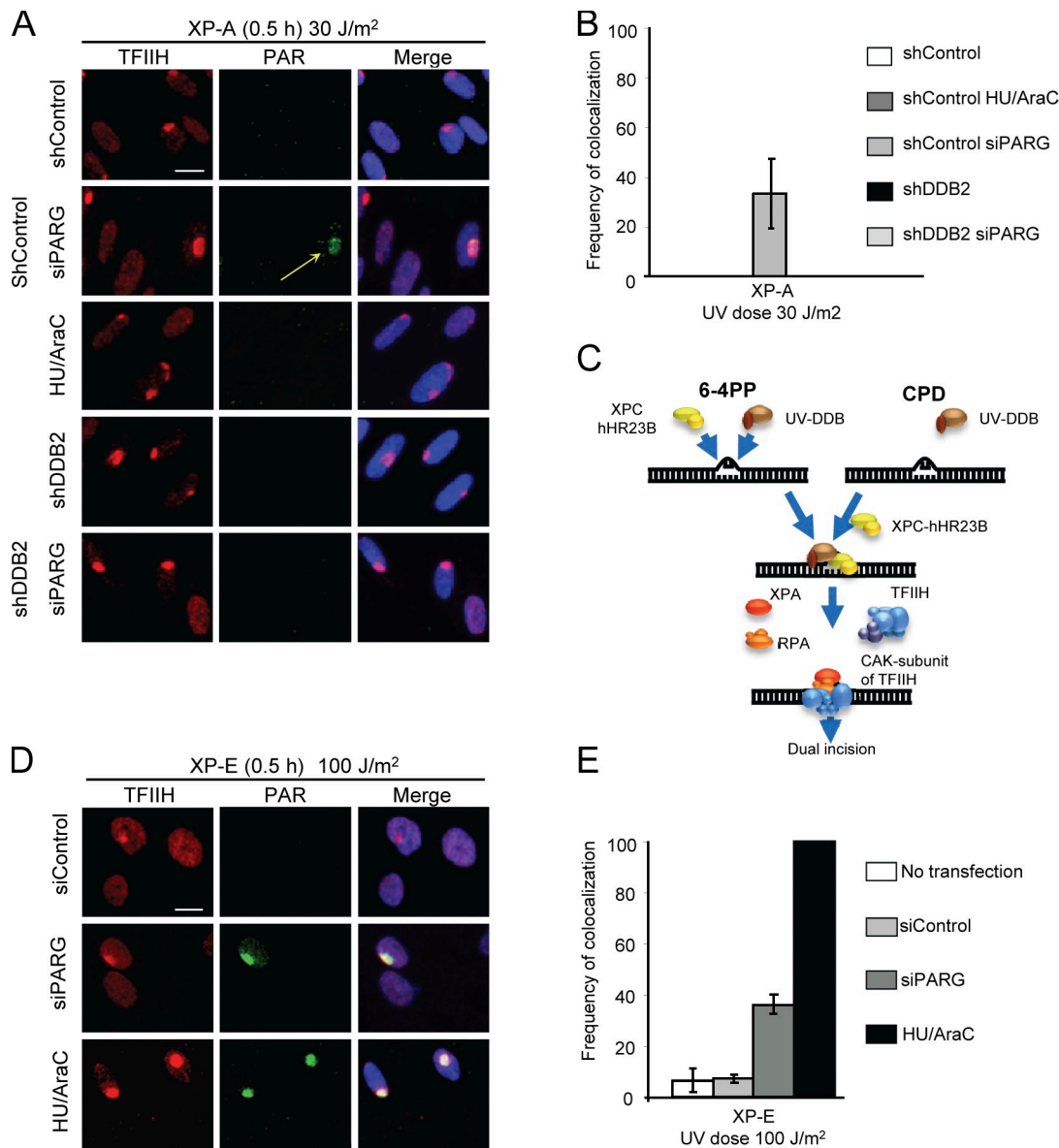
Figure 3. Knockdown of PARG and DNA repair synthesis inhibition modulate UV-dependent PARylation. (A) XP-A cells expressing shControl or shDDB2 were transfected with the indicated siRNA or treated with HU/AraC. 48 h after transfection, the cells were locally exposed to 30 J/m², fixed after the indicated time, and stained with an antibody recognizing PAR or TFIIH. The arrow indicates PAR chain synthesis at sites of local damage. (B) The percentage of colocalization of PAR with TFIIH in XP-A cells expressing shControl or shDDB2 is plotted for the different siRNA transfections and HU/AraC treatment. The results are from three independent experiments in which about 100 cells per condition were analyzed. (C) Scheme of the early stage of NER. (D) XP-E cells were transfected with indicated siRNA or treated with HU/AraC. The cells were locally UV exposed with 100 J/m², fixed after the indicated time, and stained with an antibody recognizing PAR or TFIIH. Bars, 20 µm. (E) The percentage of colocalization of PAR with TFIIH in XP-E cells is plotted for the different siRNA transfections and HU/AraC treatment. The data shown are from a single representative experiment out of three repeats. (B and E) Error bars indicate SD.

6-4PPs under the conditions described in Fig. 3 (Moser et al., 2005; Nishi et al., 2009), and all of these repair events (in the presence of HU/AraC) provoke PAR synthesis although the absolute number of events is lower than in NHFs.

We then took advantage of the finding that DDB2 is very rapidly recruited to UV-induced DNA lesions (Luijsterburg et al., 2007) compared with the assembly rates of the preincision factors and especially those of the postincision factors (Luijsterburg et al., 2010). We therefore examined PAR synthesis very shortly after UV exposure when DDB2 readily accumulates but PCNA recruitment cannot yet be detected (Luijsterburg et al., 2010).

At 5 min after UV irradiation (30 or 100 J/m²), we could not detect PAR synthesis in normal human, XP-A, or XP-E fibroblasts, not even when DNA synthesis was inhibited by HU/AraC treatment (Fig. 4). Strikingly, whereas the stabilization of PAR chains by PARG depletion (Fig. S3 E) resulted in clearly detectable PARylation at UV-damaged regions in wild-type and XP-A fibroblasts (Fig. 4, A–E), PAR synthesis at these early time points was completely abolished in XP-E cells even at 100 J/m² (Fig. 4, B–D). Collectively, our results suggest that two temporally distinct waves of PARylation take place at sites of UV-induced DNA damage. The early (preincision)
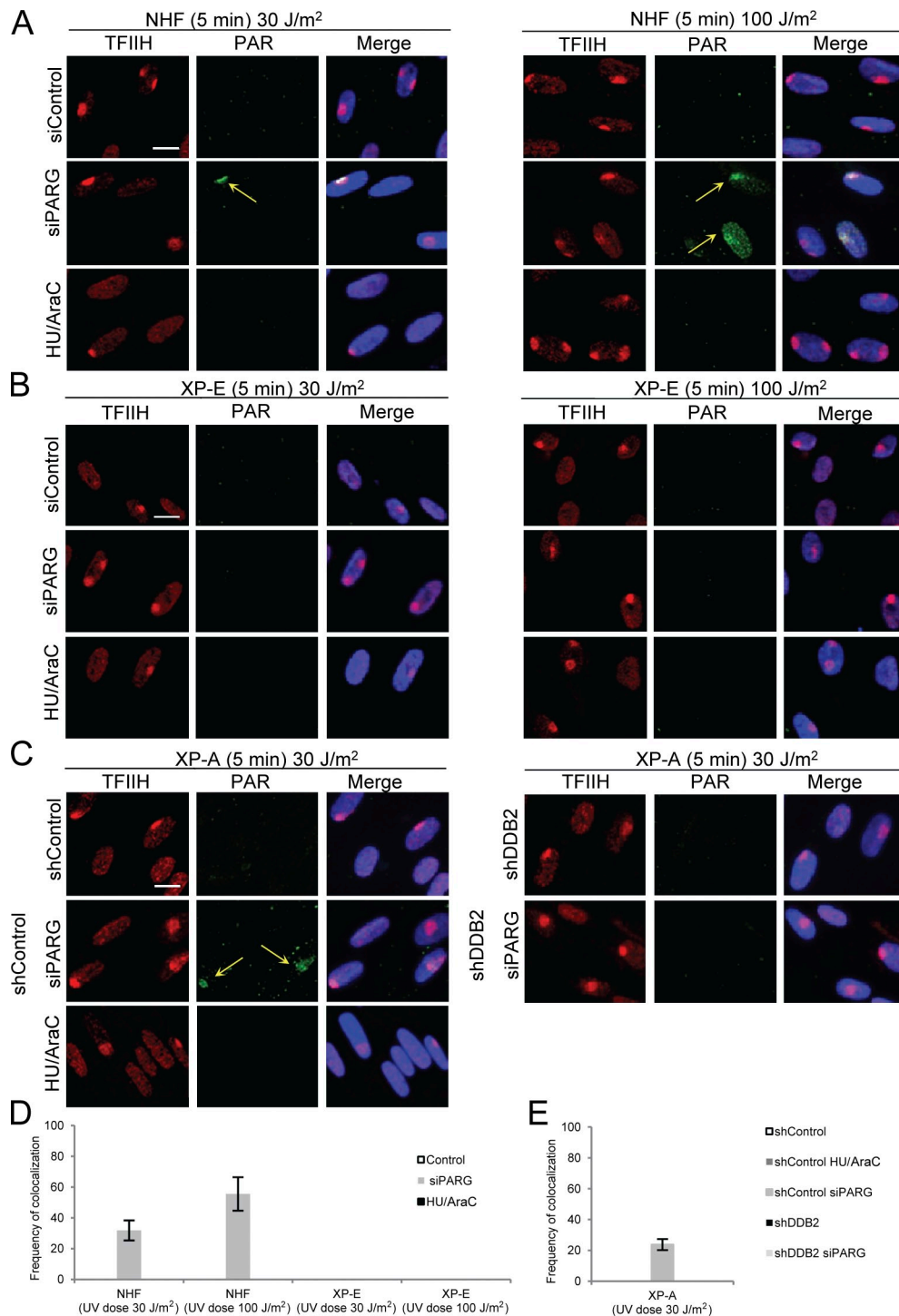
Figure 4. **DDB2 mediates PARylation.** (A and B) NHF (A) and XP-E (B) cells were transfected with the indicated siRNA or treated with HU/AraC. 48 h after transfection, the cells were locally UV exposed with 30 or 100 J/m², fixed after the indicated time, and stained with an antibody recognizing PAR or TFIIH. (C) XP-A cells expressing shControl or shDDB2 were transfected with the indicated siRNA or treated with HU/AraC. 48 h after transfection, the cells were locally UV exposed to 30 J/m², fixed after the indicated time, and stained with an antibody recognizing PAR or TFIIH. (A and C) Arrows indicate PAR chain synthesis at sites of local damage. Bars, 20 µm. (D) The percentage of colocalization of PAR with TFIIH in NHF and XPE cells is plotted for the different siRNA transfections and HU/AraC treatment. (E) The percentage of colocalization of PAR with TFIIH in XP-A cells expressing shControl or shDDB2 is plotted for the different siRNA transfections and HU/AraC treatment. The data shown are from a single representative experiment out of three repeats. (D and E) The results are from three independent experiments in which about 100 cells per condition were analyzed. Error bars indicate SD.

wave of PAR synthesis is fully dependent on functional DDB2, whereas the late (postincision) wave of PAR formation requires the generation of ssDNA gaps resulting from dual incision. In concordance, we found that PAR synthesis was completely abolished in DDB2-depleted XP-A cells even when PARG was depleted (Fig. 3, A and B; Fig. 4, C–E; and Fig. S3 C).
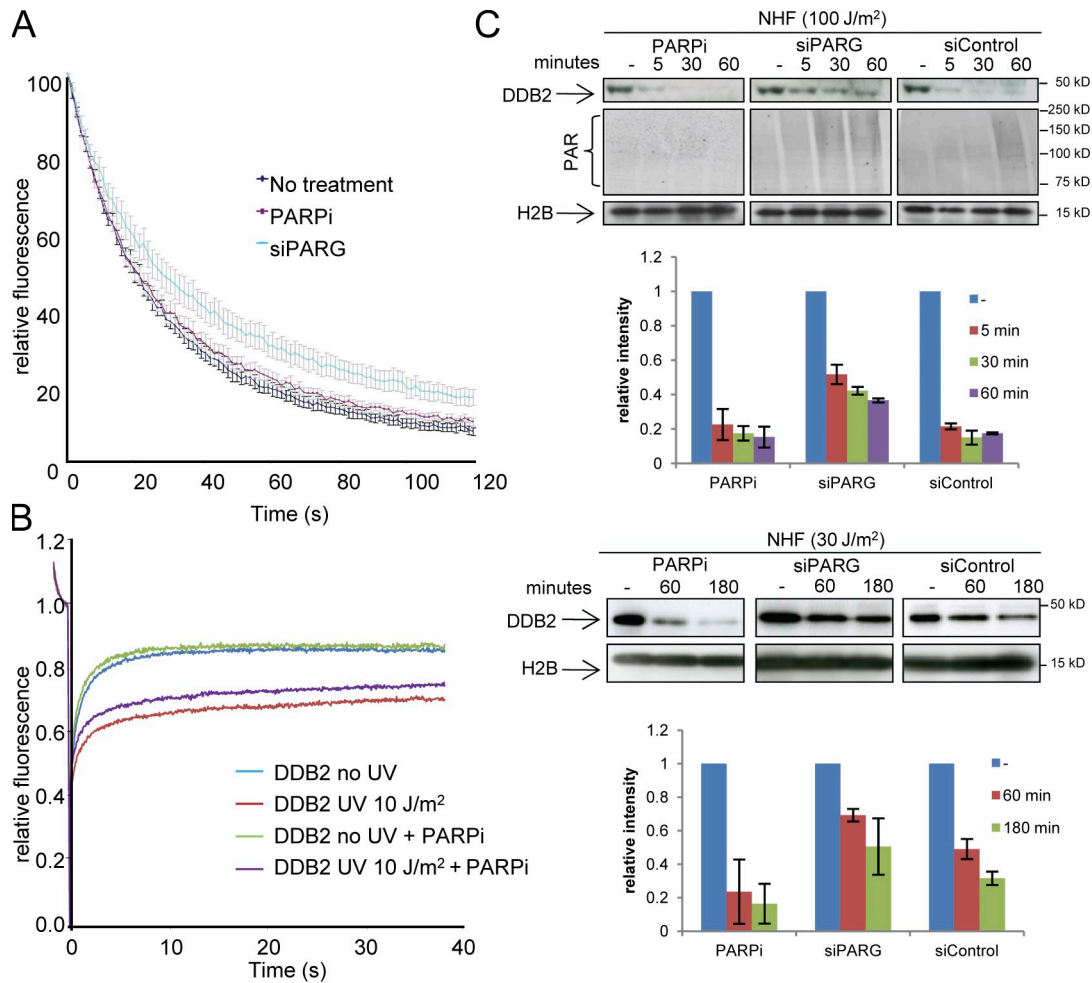
Figure 5. **PARylation affects the retention of DDB2 on UV-damaged chromatin.** (A) NHF cells stably expressing GFP-DDB2 were transfected with the indicated siRNA or treated with 10 µM PARPi. 48 h after transfection, cells were UV irradiated using a 266-nm UV-C laser. To determine the dissociation kinetics of DDB2 from UV-damaged DNA, the undamaged nucleus was continuously bleached and the fluorescence decrease in the local damage was monitored. Relative fluorescence was normalized at 100% (before bleach at maximum level of accumulation). The half-time ($t_{1/2}$) of a FLIP curve corresponds to the residence time of a protein molecule in the locally damaged area. Error bars indicate SEM. (B) VH10-tert cells stably expressing GFP-DDB2 were incubated in CO_2-independent microscopy medium supplemented with 1% DMSO (mock treatment) or 10 µM PARP inhibitor dissolved in DMSO 3 h before FRAP analysis. Cells were mock treated or globally UV-C irradiated (10 J/m^2) and transferred to the microscope chamber in microscopy medium. Cells were incubated on the microscope chamber at 37° for 10 min to allow repair proteins to accumulate at UV-induced DNA lesions after which the mobility of GFP-tagged NER factors was analyzed by strip-FRAP. The data were normalized to the prebleach intensity (set to 1) and bleach depth (set to 0). Three independent experiments were performed for each condition. (C) Western blot of normal fibroblasts transfected with the indicated siRNA or treated with 10 µM PARPi. Whole cell extracts of nonirradiated and UV-irradiated cells (30–100 J/m^2) after the indicated time were probed with antibodies against DDB2, PAR, or H2B. Error bars indicate SD.

PARylation regulates DDB2 release from UV-induced DNA lesions

To gain insight into the role of PARylation in NER complex formation, we investigated the assembly kinetics of GFP-tagged DDB2 at UV-C laser–induced DNA lesions. The kinetics of GFP-DDB2 accumulation was not affected by PARP inhibition (PARPi) or depletion of PARG (Fig. S2, A and B), indicating that the recruitment of DDB2 is not regulated by PAR chains. We subsequently applied fluorescence loss in photobleaching (FLIP) to measure the dissociation rate of DDB2 from UV-damaged DNA. Although the dissociation of DDB2 ($t_{1/2}$ = 19 s) was not affected by PARPi, we measured a prolonged chromatin retention time ($t_{1/2}$ = 27 s) upon knockdown of PARG (Fig. 5 A), suggesting that PAR synthesis positively affects the retention of DDB2 on UV-damaged chromatin.

Likewise, the immobilization of GFP-DDB2 after global UV irradiation, as measured by FRAP, was significantly reduced after treatment with PARP inhibitors (Fig. 5 B), suggesting that PAR synthesis positively affects the retention of DDB2 on UV-damaged chromatin. Consistent with these findings, Western blot analysis revealed that the UV-induced degradation of DDB2 was significantly retarded by PARG depletion (Fig. 5 C) when cells were exposed to a UV dose (100 J/m^2) comparable with the UV laser treatment (Fig. 5 A). Inhibition of PARP activity resulted in accelerated degradation of DDB2 after UV irradiation most clearly seen at 30 J/m^2. This result indicates that PARylation of DDB2 affects its UV-induced degradation presumably by affecting ubiquitylation. To address how PARylation modulates the chromatin binding and stability of DDB2, we biochemically examined whether
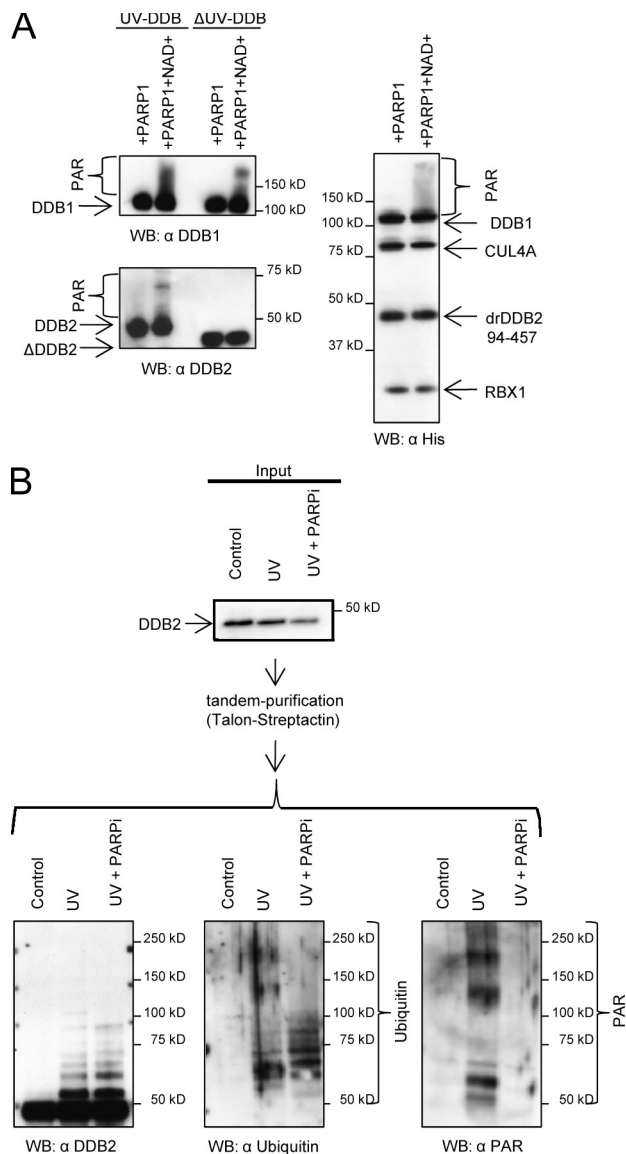
Figure 6. **DDB2 is a target for PARP1-mediated PARylation.** (A) The N terminus of DDB2 is targeted for PARylation. In vitro PARylation experiments using purified components reveal that both DDB2 and DDB1 are directly modified by PARP1. Human DDB2 lacking its first 40 N-terminal amino acids including 7 lysines (ΔUV-DDB), failed to undergo PARylation. The zebrafish orthologue of DDB2 (drDDB) lacking the first 93 N-terminal residues is also not PARylated in vitro. (B) 6His StrepII-tag DDB2 isolation using tandem purifications under denaturing conditions. NHF cells stably expressing 6His StrepII-tag DDB2 were irradiated with 100 J/m² UV-C light in the presence or absence of 10 µM PARPi or mock irradiated and incubated for 30 min. The final Strep-Tactin column purifications were separated on SDS-PAGE gels, and proteins were visualized with antibodies against DDB2, PAR, or Ubiquitin. WB, Western blot.

UV-DDB is modified by PARP1. In vitro PARylation experiments using purified components revealed that both DDB2 and DDB1 are directly modified by PARP1 (Fig. 6 A and Fig. S2 C). Conversely, human DDB2 lacking its first 40 N-terminal amino acids including 7 lysines (Fischer et al., 2011) failed to undergo PARylation (Fig. 6 A). This finding was further substantiated by the lack of in vitro PARylation of the zebrafish orthologue of DDB2 (drDDB2) lacking the first 93 N-terminal residues (Scrima et al., 2008), showing that the N terminus of

DDB2 is targeted for PARylation. Both Cul4A and Rbx1 were not modified by PARP1 (Fig. 6 A), suggesting that DDB1 and DDB2 are specific targets of PARP1. To assess PARylation of DDB2 in vivo, we expressed double-tagged DDB2 in human cells followed by its isolation using two consecutive purifications under denaturing conditions to disrupt protein–protein interactions while preserving posttranslational modifications (Fig. 6 B). Using this purification approach, we detected robust PARylation of DDB2 in response to UV irradiation, whereas PARylation was virtually absent in mock-treated cells, showing that DDB2 is modified in a DNA damage–specific manner. Strikingly, inhibition of PARP activity, which resulted in suppressed DDB2 PARylation, was accompanied by increased level and altered spectrum of ubiquitylation of DDB2 (Fig. 6 B). However, it is obvious that lysine residues on the N terminus of DBB2 are the major target of ubiquitylation (Fischer et al., 2011), and these might have more impact on DDB2 degradation than modification of lysine residues toward the C terminus when PARP activity is inhibited. These findings identify DDB2 as a novel target for PARP1-mediated PARylation and suggest that poly(ADP-ribosyl)ation of DDB2 directly suppresses DDB2 autoubiquitylation, providing a molecular explanation for the PAR-dependent stabilization of DDB2 in response to UV irradiation.

DDB2-dependent and -independent recruitment of the chromatin-remodeling enzyme ALC1 to UV-induced photolesions

Recent studies uncovered that PAR chains mediate the recruitment of PAR-binding proteins to single-stranded and double-stranded DNA breaks (Ahel et al., 2009; Gottschalk et al., 2009; Timinszky et al., 2009). In particular, the macrodomain-containing chromatin-remodeling enzyme ALC1 promotes PAR-dependent nucleosome remodeling in vitro and is recruited to sites of DNA breaks, which prompted us to test whether ALC1 is involved in the repair of UV-induced DNA lesions. Staining with a specific antibody revealed that endogenous ALC1 was readily recruited to UV-induced DNA lesions shortly after UV exposure (Fig. 7 A). Live cell imaging of GFP-tagged ALC1-expressing cells confirmed the rapid, but transient recruitment of ALC1 to sites of UV-C laser–induced DNA damage (Fig. 7 B). GFP-ALC1 was rapidly recruited to UV-induced DNA lesions in wild-type (Fig. S3 B) and XP-A cells (Fig. 7 B) shortly after exposure to the UV-C laser and could be completely suppressed by addition of the PARPi (Fig. S3 A). Strikingly, knockdown of DDB2 significantly reduced the recruitment of GFP-ALC1 in XPA-deficient cells (Fig. 7 B), as well as in repair-proficient cells at early time points after UV irradiation (Fig. S3 B), suggesting an important role for DDB2 in the recruitment of chromatin remodeler ALC1 through PARP1-mediated PAR synthesis. Consistent with our findings that two mechanistically distinct PARylation waves exist in response to UV irradiation, we found that ssDNA gaps also triggered robust GFP-ALC1 recruitment at later time points after UV irradiation in normal human as well as in XP-E cells (Fig. S4), whereas recruitment of ALC1 was absent in dual incision–defective XP-A cells not even in the presence of HU/AraC (Fig. S4). In contrast, the
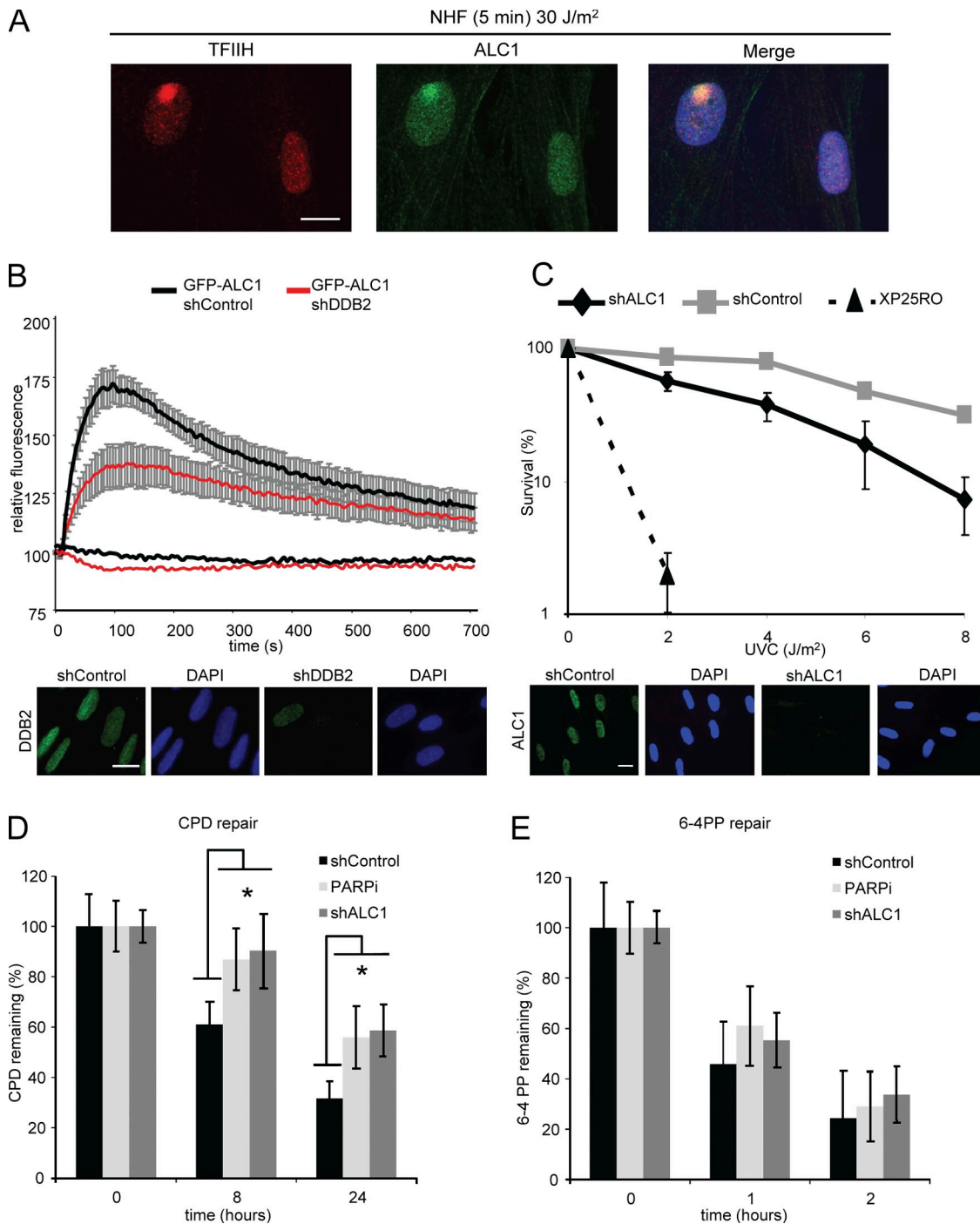
Figure 7. **DDB2-dependent recruitment of ALC1 to UV lesions.** (A) NHF cells were locally UV irradiated (100 J/m²), fixed after the indicated time, and stained with an antibody recognizing ALC1 or TFIIH. ALC1 colocalizes with the damage marker TFIIH. (B) XP-A cells stably expressing GFP-ALC1 were infected with the indicated shRNA. The cells were UV damaged using UV-C (266 nm) laser irradiation. GFP fluorescence intensities at the site of UV damage were measured by real-time imaging until they reached a maximum. Assembly kinetic curves were derived from at least six cells for each protein. Error bars indicate SEM. (C) Clonal survival of UV-irradiated NHF cells expressing shControl or shALC1 and XPA cells. The percentage of surviving cells is plotted against the applied UV-C dose (J/m²). The results are from three independent experiments. Error bars indicate SD. Bars, 20 μm. (D) NHF cells expressing shControl or shALC1 RNAi or treated with 10 μM PARPi were irradiated with 10 J/m² UV-C, fixed immediately, at 8 or 24 h after UV treatment, and stained with anti-CPD antibody (*, P < 0.05, analysis of variance). (E) NHF cells expressing shControl or shALC1 or treated with 10 μM PARPi were irradiated with 10 J/m² UV-C, fixed immediately, at 1 or 2 h after UV treatment, and stained with an anti–6-4PP antibody. The total fluorescence intensity of the nucleus was quantified and divided by the surface area, resulting in a specific fluorescence intensity expressed in arbitrary units. Values are the result of three independent experiments (100 cells per time point). (D and E) Error bars indicate SD.

stabilization of PAR chains by PARG depletion (Fig. S4) resulted in clearly detectable GFP-ALC1 recruitment at UV-damaged regions in XP-A fibroblasts. In summary, our results reveal that the chromatin-remodeling enzyme ALC1 is recruited to PAR chains synthesized during repair by NER through distinct molecular mechanisms.

PARP1 inhibition and ALC1 depletion impair CPD repair and render cells sensitive to UV irradiation

Having established that ALC1 is recruited to sites of local damage, we subsequently addressed the biological impact of this finding. To this end, we generated a cell line stably expressing a short hairpin RNA (shRNA) targeting endogenous ALC1. Knockdown of ALC1 rendered cells sensitive to UV irradiation compared with control cells (Fig. 7 C), indicating that ALC1 protects cells against UV-induced cytotoxicity. Likewise, chemical inhibition of PARP also rendered cells UV sensitive (Fig. S3 D), underscoring an important role for PAR synthesis in NER. Finally, we directly measured the repair of UV-induced DNA lesions after a UV dose of 10 J/m^2 by immunostaining using antibodies against 6-4PPs or CPDs. While the repair of 6-4PPs was not significantly affected, we measured a significant reduction in CPD repair upon ALC1 depletion or chemical inhibition of PARP1 (Fig. 7, D and E). Corroborating these findings, an ELISA-based assay confirmed that knockdown of ALC1 conferred a significant reduction in CPD repair (Fig. S5). These findings reveal an unanticipated role of PAR synthesis and ALC1 in efficient repair of CPDs by human NER.

Discussion

Despite detailed insights into the NER reaction and the core proteins involved (Gillet and Schärer, 2006; Sugasawa, 2010), the regulatory pathways that govern NER activity in living cells are still poorly understood. Among others, these pathways involve the posttranslational modifications of NER proteins and the activity of chromatin-remodeling enzymes to optimize repair of DNA damage embedded in chromatin. DDB2 is the first NER factor to be recruited to UV-induced DNA lesions (Luijsterburg et al., 2007) and it regulates NER by direct DNA lesion recognition (Scrima et al., 2008) and modulation of chromatin structure (Palomera-Sanchez and Zurita, 2011). We identified PARP1 as a novel DDB2-associated factor in UV–irradiated cells. The fact that the interaction between these factors occurred in nondividing UV-irradiated human fibroblasts excludes the possibility that involvement of PARP1 in NER is merely related to the stalling of replication forks (Bryant et al., 2009). Although we found PARP1 as a novel DDB2-associated factor, in vitro assays with purified proteins revealed that PARP binds to both DDB1 and DDB2 but with higher preference for DDB2.

We found robust synthesis of PAR chains in nuclear regions containing UV-induced DNA lesions that was completely suppressed by chemical PARPi. These findings directly link PARP1 to the repair of photolesions and fit with previous observations that UV irradiation triggers both stimulation of PAR synthesis (Cleaver et al., 1983) and association of PARP1 with UV photolesions in chromatin (Vodenicharov et al., 2005). Although these findings clearly implicate PARP1 activity in response to UV irradiation, we and others (Schultz et al., 2003; Bryant et al., 2009) failed to detect the recruitment of endogenous PARP1 to UV-induced DNA lesions or UV-induced stalled replication forks, which is possibly because of the transient

nature of its interaction or the abundance of PARP1 in the nucleus (Krishnakumar and Kraus, 2010).

Our study identified two distinct molecular mechanisms that orchestrate the synthesis of PAR chains at UV-induced DNA damage. First, we show that persistent ssDNA gaps generated by inhibition of repair synthesis elicit DDB2-independent PARylation at NER sites. However, a possible role of PARylation in regulation of postincision repair has not yet been dissected, although recruitment of postincision factor XRCC1, disassembly kinetics of NER complexes (Moser et al., 2007), or sealing of UV-induced ssDNA gaps was not impaired by PARPi (Cleaver et al., 1983). Second and more importantly, we show that DDB2 regulates fast and transient PARylation at sites of UV-induced DNA damage during the preincision stage of NER. One target of PARylation is DDB2 itself as shown by PARylated DDB2 purified from UV-irradiated cells. It is likely that this modification underlies among others the UV-specific occurrence of DDB2 peptides of >50-kD molecular mass in immunoprecipitates of chromatin-bound DDB2. The initial DDB2-mediated wave of PAR synthesis does not require incision and is regulated by the activity of PARG. Indeed, there is increasing evidence that DNA breaks are not an absolute requirement for PARP1 activation (Krishnakumar and Kraus, 2010). Several alternative mechanisms to activate PARP1 in the absence of DNA breaks have been proposed, including interaction with other proteins (Cohen-Armon et al., 2007) or posttranslational modifications such as phosphorylation, acetylation (Hassa et al., 2003; Rajamohan et al., 2009), SUMOylation, and ubiquitylation (Martin et al., 2009; Messner et al., 2009). In this light, it is feasible that the DDB2-associated E3 ubiquitin ligase activity (Shiyanov et al., 1999; Groisman et al., 2003) might activate PARP1. At the same time, it is possible that PARP1 activation is modulated by DDB2-mediated acetylation through its interaction with histone acetyltransferases p300 and the STAGA complex (Datta et al., 2001; Martinez et al., 2001; Rapić-Otrin et al., 2002).

Molecular mechanisms for DDB2-mediated and PARP1-executed regulation of NER

Our data provide mechanistic insights into how DDB2 promotes NER in chromatin through two novel mechanisms. On one hand, DDB2 is directly targeted by poly(ADP-ribosyl)ation and ubiquitylation (Fischer et al., 2011) in response to UV irradiation. As PARylation (Messner et al., 2010) and ubiquitylation are targeted to lysine and both modifications appear to occur in the same N-terminal region of DDB2, competition between PARylation and ubiquitylation of target lysine residues might constitute an important mechanism of DDB2-mediated regulation of NER. The in vivo data support a competition model in which the poly(ADP-ribosyl)ation of DDB2 results in increased protein stability and a prolonged chromatin retention time on the UV lesion. At the same time, poly(ADP-ribosyl)ation of DDB2 suppresses its UV-induced ubiquitylation and consequently leads to reduced degradation of DDB2. Together our data disclose a mechanism by which two opposing modifications regulate the steady-state levels and retention time of DDB2 at sites of UV photolesions.

On the other hand, DDB2-dependent PARylation events also stimulate the preincision step of NER. We show that DDB2-dependent PARylation through PARP1 at UV-induced DNA lesions targets chromatin remodeler ALC1 to these sites. ALC1 belongs to the Swi2/Snf2 ATPase superfamily and through its macrodomain interacts transiently with chromatin that is modified by PARP1. We propose that these protein modifications serve to locally modulate chromatin structure through PARP1-stimulated nucleosome sliding to promote NER (Ahel et al., 2009; Gottschalk et al., 2009). Consistent with this scenario, we show that loss of ALC1 or chemical inhibition of PARP1 resulted in defects in the repair of CPDs concomitantly with increased sensitivity to UV exposure, underscoring the importance of the DDB2–PARP1–ALC1 pathway in promoting NER. We noted that the defects in CPD repair caused by loss of ALC1 or PARP1 activity are less pronounced than repair defects caused by loss of DDB2 (Pines et al., 2009), suggesting that the essential role of DDB2 in CPD repair is not solely caused by its recruitment of PARP1-mediated activities, but also involves other functions of DDB2 such as its ubiquitin ligase activity. Interestingly, XPC contains a putative PAR-binding sequence (Gagné et al., 2008), suggesting that UV-DDB–dependent PARylation may promote the accessibility of UV lesions through remodeling of the chromatin structure as well as providing an enhancer signal for the recruitment of preincision NER proteins.

A model of DDB2- and PARP1-dependent regulation of NER

The high affinity of DDB2 for DNA and its preference for UV-damaged DNA makes UV-DDB the most important DNA damage recognition factor for 6-4PPs and CPDs (Wittschieben et al., 2005). UV-DDB is the first NER factor to be recruited to UV damage (Luijsterburg et al., 2007; Nishi et al., 2009) as part of the Cullin-RING ubiquitin ligase (CRL4) complex CUL4A–RBX1 (Fig. 7). As shown for 6-4PPs (Scrima et al., 2008), the CUL4A–RBX1 complex binds to photolesions by the WD40 domain of DDB2 and in concert with PARP1 tightly regulates steady-state levels and retention time of DDB2 by opposing modifications (PARylation and ubiquitylation) of the same N-terminal region of DDB2. The enhanced extension time of PARylated DDB2 on UV damage might be particularly important for CPD photolesions that induce much less disruption of base pairing interactions than 6-4PPs (Kim and Choi, 1995) and fully depend on functional DDB2 for their repair. Purified (non-PARylated) DDB2 recognizes CPDs and 6-4PPs with a 5- and 80-fold higher affinity, respectively, than nondamaged DNA (Wittschieben et al., 2005); this affinity of DDB2 for CPDs might be too low for productive repair, i.e., recruitment of XPC. We speculate that extended binding of PARylated DDB2 to CPDs will provoke the induction of chromatin modifications at the site of DNA damage to allow productive interaction and ubiquitylation of XPC and UV-DDB required for NER (Sugasawa et al., 2005). Underscoring the importance of PAR synthesis in the assembly of the preincision NER complex, we found that PARPi leads to reduced recruitment of the preincision factor XPC as shown in our recent work (Luijsterburg et al., 2012), whereas depletion of PARG stimulates binding of

XPC (Luijsterburg et al., 2012) and TFIIH (unpublished data). Whether UV-DDB activates PARP1 through its E3 ubiquitin ligase activity or whether PARP1 activation occurs in parallel with or precedes ubiquitylation is not clear. PARP1-mediated increase of retention time of DDB2 at UV damage and DDB2 protection by suppressing its ubiquitylation-dependent degradation argue for PARylation as the initiating event. Moreover, PARP1 might create accessibility for recruitment of NER factors by its ability to disrupt chromatin structure by PARylation of histones and destabilizing nucleosomes (Krishnakumar and Kraus, 2010). Additionally PARylation of chromatin effectuates recruitment of NER-promoting factors such as the Swi2/Snf2 chromatin remodeler ALC1 to UV-damaged DNA to locally modulate chromatin structure through nucleosome sliding (Fig. 8), thereby stimulating the recruitment of XPC to assemble a functional repair complex. Our study also identified DDB2-independent PARylation and recruitment of ALC1 at NER sites that is trigged by transient ssDNA gaps generated by the dual incision step of NER (Fig. 8); this process of PARylation is amplified by inhibition of DNA repair synthesis. The role of PARylation and ALC1 in regulation of the postincision step of NER remains to be resolved.

Materials and methods

Cell culture and UV-C irradiation
The following cell lines were used for this study: VH10 hTert (NHF), XP25RO hTert (XP-A), GM01389 hTert (XP-E), U2OS, and MRC5 fibroblasts. Cells were grown in DME supplemented with 10% fetal calf serum, penicillin, and streptomycin. 2 d before experiments, medium was changed to DME supplemented with 0.2% serum fetal calf serum, penicillin, and streptomycin. UV irradiation of cells was carried out using a 254-nm UV-C source. Local irradiation was performed using 5-µm filters as described previously (Volker et al., 2001). UV lamp–induced damage was inflicted using a 254-nm UV source (TUV PL-S 9W; Philips). For induction of global UV damage, cells were rinsed with PBS and irradiated with 8 or 16 J/m². For induction of local UV damage, cells were UV irradiated through a polycarbonate mask (Millipore) with pores of 8 µm and subsequently irradiated with 30 or 100 J/m². The AZ12640831-009 PARPi was used at a final concentration of 10 µM and was a gift from AstraZeneca. Cells were pretreated 30 min before irradiation.

Generation of cell lines
ALC1 and DDB2 cDNA were cloned into vector pENTR4-GFP-C1 (E. Campeau, University of Massachusetts Medical School, Worcester, MA; Addgene: w392-1) and were subsequently recombined into pLenti6.3 V5-DEST (Invitrogen) using gateway recombination. VH10 hTert or XP25RO hTert fibroblasts were transduced with pLenti6.3 GFP-ALC1 or pLenti6.3 GFP-DDB2 lentiviral particles and cultured with 5 µg/ml blasticidin (InvivoGen) to select for integrands.

For DDB2 isolation, a 6His and StrepII-tag were fused to the N terminus of DDB2. A synthetic oligonucleotide coding for 6His StrepII-tag was inserted into pENTR4 (Invitrogen), and DDB2 cDNA was subsequently cloned in. Lentiviral particles were generated after recombination of this vector to pLenti6.3 V5-DEST and used for transducing VH10 hTert cells.

NHFs and XP-A fibroblasts stably expressing shRNA were generated by lentiviral transduction of control, ALC1, or DDB2 targeting constructs followed by 1 µg/ml puromycin selection. The following shRNA vectors were used: TRCN0000013471 (ALC1) TRCN0000083995 (DDB2), and SHC002 (nontargeting control) from the RNAi Consortium (Sigma-Aldrich).

RNA interference
siRNA duplexes used were as follows: SMARTpool siRNA targeting the PARG transcript and SMARTpool nontargeting siRNA (Thermo Fisher Scientific). Cells were transfected using HiPerFect (QIAGEN) according to the

Figure 8. A model of DDB2- and PARP1-dependent regulation of NER. UV-DDB is the first NER factor to be recruited to UV damage as part of the Cullin-RING ubiquitin ligase (CRL4) complex CUL4A–RBX1. This complex binds to UV damage, and both DDB1 and DDB2 might be involved in binding of PARP1. In concert with PARP1, the CUL4A–RBX1 complex tightly regulates steady-state levels and retention time of DDB2 by opposing modifications (PARylation and ubiquitylation) of the same N-terminal region of DDB2. Additionally, PARP1-dependent PARylation of chromatin also effectuates recruitment of the Swi2/Snf2 chromatin remodeler ALC1 to UV-damaged DNA to locally modulate chromatin structure through nucleosome sliding, thereby stimulating the recruitment of XPC. The second distinct waves of PARylation and ALC1 recruitment require the generation of ssDNA gaps resulting from dual incision.
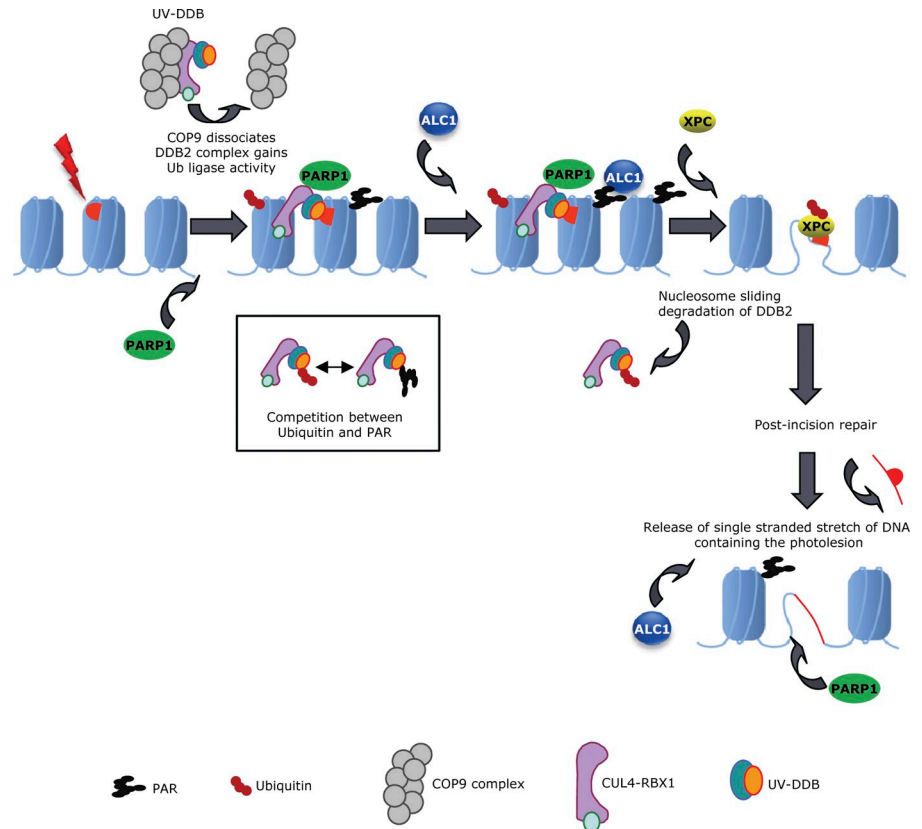
manufacturer's protocol. For PARG knockdown, two sequential transfections were performed. Immunostaining and Western blot experiments were performed 48 h after the final transfection.

Complex isolation

Isolation of the DDB2 complex was performed according to published procedures with some modifications (Groisman et al., 2003). In brief, cells were irradiated with UV-C at 20 J/m^2 and incubated for 5 min. To prepare nuclear extracts, cells were suspended in hypotonic buffer (10 mM Tris-HCl, pH 7.3, 10 mM KCl, 1.5 mM MgCl$_2$, 10 mM β-mercaptoethanol, and 0.2 mM PMSF) and disrupted by Dounce homogenization. Nuclei were collected by centrifugation at 2,000 g for 15 min at 4°C and resuspended in extraction buffer (15 mM Tris-HCl, pH 7.3, 1 mM EDTA, 0.21 M NaCl, 1 mM MgCl$_2$, 10% glycerol, 10 mM β-mercaptoethanol, and 0.2 mM PMSF). After incubating on ice for 30 min, the samples were centrifuged at 20,000 g for 30 min at 4°C, and the supernatant was used as the nuclear extract fraction. The nuclear pellet fraction was washed and resuspended in the micrococcal nuclease buffer (20 mM Tris-HCl, pH 7.5, 100 mM KCl, 2 mM MgCl$_2$, 1 mM CaCl$_2$, 0.3 M sucrose, 0.1% Triton X-100, and complete protease inhibitor cocktail [Roche]). Micrococcal nuclease was added at 3 U/ml, and the samples were incubated for 10 min at room temperature, whereupon the reaction was terminated by adding 5 mM EGTA and 5 mM EDTA. The samples were centrifuged at 2,000 g for 5 min at 4°C, and the supernatant was used as the solubilized chromatin fraction. The UV-DDB complex was immunoprecipitated from solubilized chromatin prepared from MRC5 cells expressing FLAG-DDB2 by incubating with M2 anti-FLAG agarose overnight with rotation. After an extensive wash with wash buffer (0.1 M KCl, 20 mM Tris-HCl, pH 8.0, 5 mM MgCl$_2$, 10% glycerol, 1 mM PMSF, 0.1% Tween 20, and 10 mM β-mercaptoethanol), the bound proteins were eluted from M2 agarose by incubation for 30 min with FLAG peptide (0.2 mg/ml in PBS). The elution procedure was repeated three times.

In-gel tryptic digestion

Immunoprecipitates were separated on SDS-PAGE gels, and proteins were visualized with Coomassie (SimplyBlue; Invitrogen). Gel lanes were sliced into 25–30 bands, cut into small pieces, and washed with 25 mM NH$_4$HCO$_3$ followed by two rounds of dehydration with 100% acetonitrile for 10 min. For reduction and alkylation, gel particles were first incubated with 10 mM dithiothreitol for 30 min at 56°C. Following dehydration with acetonitrile, gel plugs were subsequently incubated in 55 mM iodoacetamide for 20 min at room temperature. After two rounds of washing with 25 mM NH$_4$HCO$_3$ and dehydration with 100% acetonitrile, the gel particles were completely dried in a centrifugal vacuum concentrator (Eppendorf). Dried gel particles were re-swollen for 15 min on ice by addition of 15 µl of a trypsin solution (12.5 ng/µl in 25 mM NH$_4$HCO$_3$; sequencing-grade modified trypsin; Promega). After this, 20 µl of 25 mM NH$_4$HCO$_3$ was added, and samples were kept on ice for an additional 30 min. Tryptic digestion was subsequently performed overnight at 37°C. After tryptic digestion, the overlaying digestion solution was collected. Two additional rounds of extraction with 20 µl of 0.1% TFA were used to extract peptides from the gel plugs, and all extracts were pooled.

Nano liquid chromatography (LC) electrospray ionization MS/MS

Nanoflow LC was performed on an Ultimate LC system (Dionex). A volume of 10 µl of sample was injected onto a C18 PepMap 0.3 mm × 5 mm trapping column (Dionex) and washed with 100% A (2% acetonitrile in 0.1% formic acid in MQ water [vol/vol]) at 20 µl/min for 15 min. After valve switching, peptides were separated on a C18 PepMap 75 µm × 150 mm column (Dionex) at a constant flow of 200 nl/min. The peptide elution gradient was from 10 to 60% B (95% acetonitrile in 0.1% formic acid in MQ water [vol/vol]) over 50 min. The nanoflow LC system was coupled to an HCTultra IonTrap (Bruker Daltonics) using a nano-electrospray ionization source. The spray voltage was set at 1.2 kV, and the temperature of the heated capillary was set to 165°C. Eluting peptides were analyzed using the data-dependent MS/MS mode over a 300–1,500 m/z range. The five most abundant ions in an MS spectrum were selected for MS/MS analysis by collision-induced dissociation using helium as the collision gas.

MS data analysis

Peak lists were generated using DataAnalysis 4.0 software (Bruker Daltonics) and exported as Mascot Generic (MGF) files. These files were searched against the human IPI database using the Mascot (version 2.2.1) search algorithm (Matrix Science). An MS tolerance of 0.6 Da (with # 13C = 1) and an MS/MS tolerance of 0.5 Da were used. Trypsin was designated as the enzyme, and up to one missed cleavage site was allowed. Carbamidomethyl cysteine was selected as a fixed modification and oxidation of methionine as a variable modification.

Immunofluorescent labeling (IF) and Western blotting (WB)

The cells were fixed with methanol/acetone (50%/50%) for 10 min at 4°C. After an extensive wash with PBS, the cells were incubated for 60 min at room temperature with buffer containing 0.5% BSA and 0.05% Tween 20 in PBS. Antibody incubations were performed at room temperature, and cells were counterstained with DAPI. Images were captured with an Axioplan2 microscope (Carl Zeiss) equipped with an Axiocam MRm camera (Carl Zeiss) using either a Plan-NEOFLUAR 40×/1.30 or 63×/1.25 objective. Fluorescence intensity of randomly captured images was quantified using Axiovision software (Carl Zeiss). For total extract, the cells were lysed directly in Laemmli SDS sample buffer. Western blot analysis was performed as described previously (Fousteri et al., 2006), and protein bands were visualized via chemiluminescence (ECL-Plus; GE Healthcare) using HRP-conjugated secondary antibodies or via an Odyssey Infrared Imaging System (LI-COR Biosciences) using secondary antibodies labeled with IR fluorophores (LI-COR Biosciences). The following antibodies were used: mouse α-DDB2 at 1:500 (IF) or 1:1,000 (WB; MyBioSource), mouse α-Parp1 at 1:1,000 (WB; Abnova), mouse α-PAR at 1:100 (IF and WB; Abcam), mouse α-ALC1 at 1:500 (IF) or 1:1,000 (WB; Abcam), mouse α-GFP at 1:5,000 (WB; Roche), goat α-DDB1 at 1:1,000 (WB; Abcam), goat α-DDB2 at 1:1,000 (WB; Santa Cruz Biotechnology, Inc.), rabbit α-PAR at 1:100 (IF and WB; BD), rabbit α-H2B at 1:5,000 (WB; Santa Cruz Biotechnology, Inc.), rabbit α-PARG at 1:1,000 (C-term; WB; Origene), and mouse α–6-4PP and α-CPD at 1:1,000 (IF; CosmoBio). Alexa Fluor 488– and Alexa Fluor 555–conjugated antibodies were purchased from Invitrogen.

Live cell confocal laser-scanning microscopy

Confocal laser-scanning microscopy images were obtained using a confocal microscope (LSM 510 META) with a 63× oil Plan-Apochromat 1.4 NA oil immersion lens (Carl Zeiss) equipped with a cell culture microscopy stage. GFP fluorescence imaging was recorded after excitation with a 488-nm argon laser and a 515–540-nm band-pass filter. FLIP was performed as described previously (Houtsmuller and Vermeulen, 2001; Zotter et al., 2006). Kinetics of GFP-tagged ALC1 and DDB2 accumulation were performed using UV-C (266 nm) laser irradiation as described previously (Dinant et al., 2007). In brief, VH10-tert cells stably expressing GFP-DDB2 and GFP-ALC1 were incubated in CO_2-independent microscopy medium (137 mM NaCl, 5.4 mM KCl, 1.8 mM $CaCl_2$, 0.8 mM $MgSO_4$, 20 mM D-glucose, 20 mM Hepes, and 10% FCS), and 2 mW pulsed (7.8 kHz) diode pumped solid state laser emitting at 266 nm (Rapp OptoElectronic; Hamburg GmbH) was used for local UV-C irradiation. To determine the dissociation kinetics of DDB2 from UV-damaged DNA, the undamaged nucleus was continuously bleached, and the fluorescence decrease in the local damage was monitored. Relative fluorescence was normalized at 100% (before bleach at maximum level of accumulation). The half-time ($t_{1/2}$) of a FLIP curve corresponds to the residence time of a protein molecule in the locally damaged area. Images obtained with the confocal microscope were analyzed using AIM software (Carl Zeiss). Fluorescence levels were determined for the specified region where damage was induced in addition to the complete nucleus. From these data points, the relative amount of protein in the damaged area was determined in time.

FRAP

VH10-tert cells stably expressing GFP-DDB2 were incubated in CO_2-independent microscopy medium (137 mM NaCl, 5.4 mM KCl, 1.8 mM $CaCl_2$, 0.8 mM $MgSO_4$, 20 mM D-glucose, 20 mM Hepes, and 10% FCS) supplemented with 1% DMSO (mock treatment) or 10 µM PARP inhibitor dissolved in DMSO 3 h before FRAP analysis. Cells were subsequently rinsed with PBS, mock treated or globally UV-C irradiated (10 J/m²), and transferred to the microscope chamber in microscopy medium (supplemented with DMSO or PARP inhibitor). Cells were incubated on the microscope chamber at 37°C for 10 min to allow repair proteins to accumulate at UV-induced DNA lesions, after which the mobility of GFP-tagged NER factors was analyzed by strip-FRAP. In brief, FRAP analysis was performed by bleaching (5 iterations) a narrow strip (512 × 40 pixels at zoom 8) spanning the nucleus with maximal 488-nm laser intensity (acousto-optic tunable filter 100%). The re-equilibration of bleached and nonbleached molecules was monitored in a region of 512 × 50 pixels (zoom 8) with low laser intensity (0.5% for GFP-DDB2) for at least 700 images with a 38-ms time interval between images. The data were normalized to prebleach intensity (set to 1) and bleach depth (set to 0). Three independent experiments were performed for each condition.

UV survival

Cellular survival of VH10 hTert shControl, VH10 hTert shALC1, and XP-A cells was determined using a colony assay. Cells were plated in 10-cm dishes, and after 16 h, cells were exposed to 254 nm UV-C (TUV lamp; Phillips) and left to grow for 14 d, fixed, and stained with methylene blue. Colonies were counted to assess the colony-forming ability.

In vitro poly(ADP-ribosyl)ation assay

The assay was performed according to published procedures (Deng et al., 2005) using recombinant proteins purified as described in Fischer et al. (2011).

DDB2 purification

VH10 hTert cells stably expressing 6His StrepII-tag DDB2 were irradiated with UV-C light (100 J/m²) or mock irradiated and incubated for 30 min. Cells were collected and lysed in lysis buffer (8 M urea, 2 M NaCl, 25 mM Tris, pH 8, 1 mM $MgCl_2$, and 0.2% Triton). The lysates were diluted at least seven times, after which 25 Benzonase units were added per milliliter. After incubating at room temperature for 30 min, samples were centrifuged at 16,000 g for 10 min. TALON beads (Takara Bio Inc.) were added to the supernatants and incubated for 4 h at room temperature. After an extensive wash with wash buffer (8 M urea, 25 mM Tris, pH 8, 1 mM $MgCl_2$, and 20 mM imidazole), the 6His StrepII-tag DDB2 was eluted by overnight incubation with the elution buffer (8 M urea, 25 mM Tris, pH 8, 500 mM imidazole, and 1% SDS). The elutes were concentrated by Vivaspin centrifugal concentrators (Sartorius) and diluted in Strep-Tactin buffer (100 mM Tris, pH 8, 1 mM EDTA, and 150 mM NaCl). A second purification step was performed using Strep-Tactin spin columns according to the manufacturer's protocol (IBA). Elutes were separated on SDS-PAGE gels, and proteins were visualized by Western blot.

GFP-DDB2–PARP-1 binding assay

U2OS cells transfected with GFP constructs for 24 h were lysed in denaturing buffer (20 mM Tris, pH 7.5, 50 mM NaCl, 0.5% NP-40, 1% sodium deoxycholate, 1% SDS, 1 mM EDTA, and Benzonase final concentration 0.25 U/µl) containing protease inhibitor cocktails (Roche) and subjected to immunoprecipitation with GFP-TRAP beads (Chromotek) for 1 h at room temperature. The beads were then washed extensively in a buffer (20 mM Tris, pH 7.5, 50 mM NaCl, 0.5% NP-40, 0.5% sodium deoxycholate, 0.5% SDS, and 1 mM EDTA) that disrupts protein–protein interactions, followed by two washes in EBC buffer (50 mM Tris, pH 7.5, 150 mM NaCl, 0.5% NP-40, and 1 mM EDTA), and incubated with 100 ng purified, recombinant PARP-1 (Sigma-Aldrich) for 2 h at room temperature. The beads were then washed thoroughly in EBC buffer and processed for immunoblotting.

In vitro coimmunoprecipitation

UV-DDB, ΔUV-DDB (DDB2 lacking its first 40 N-terminal amino acids), GFP, and PARP-1 recombinant protein were used to test direct interaction in vitro. The reaction volume was adjusted to 400 µl in EBC buffer (50 mM Tris, pH 7.5, 150 mM NaCl, 0.5% NP-40, and 1 mM EDTA), and 0.5 µg anti–PARP-1 antibody was added. The mixture was incubated and rotated at 4°C for 3 h. The antigen–antibody complex was captured by incubation with 15 µl of protein A–agarose beads (GE Healthcare) for 2 h in a cold room. The beads were washed extensively in EBC buffer, resuspended in 20 µl Laemmli sample buffer, and processed for immunoblotting.

Far-Western blot analysis

100 ng UV-DDB and 1,000 ng GFP recombinant proteins were separated by SDS-PAGE and transferred to a polyvinylidene difluoride membrane. The proteins on the membrane were denatured for 10 min with a 6 M guanidine hydrochloride (GuHCl) solution in HBB buffer (10 mM Hepes, pH 7.5, 60 mM KCl, 1 mM EDTA, and 1 mM DTT). Proteins were then renatured in the same HBB buffer with progressively decreasing GuHCl concentration. The membrane was rinsed extensively in HBB and blocked for 1 h in blocking buffer. After, the membrane was incubated with 10 µg/ml PARP-1 recombinant protein in HBB for 16 h. Unbound proteins were removed with extensive washes for 30 min in the same buffer. The PARP-1 binding was visualized by Western blot.

CPD/6-4PP ELISA

Cells were plated in 96-well plates, irradiated with 10 J/m² UV, and incubated for various periods to allow cells to repair DNA photolesions. The cells were fixed with methanol/acetone (50%/50%) for 10 min. After an extensive wash with PBS, the cells were incubated for 3 min at room temperature

with 10 mM NaOH. The cells were rinsed extensively in PBS and incubated for 60 min at room temperature with buffer containing 0.5% BSA and 0.05% Tween 20 in PBS. The plates were sequentially incubated with TDM-2 or 64M-2 antibodies specific for CDP or 6-4PP, respectively, and secondary antibody conjugated with HRP. After washings, substrate solution Turbo TMB-ELISA (Thermo Fisher Scientific) was added to the plates and incubated for 15–30 min. Absorbance at 490 nm was measured using a microplate reader after the addition of 2 M H_2SO_4.

Online supplemental material

Fig. S1 shows direct interaction in vitro between DDB2 and PARP-1. Fig. S2 shows that the kinetics of GFP-DDB2 accumulation was not affected by PARPi or depletion of PARG. Fig. S3 shows transient recruitment of GFP-ALC1 to sites of UV-C laser–induced DNA damage. Fig. S4 demonstrates that ssDNA gaps also triggered robust GFP-ALC1 recruitment at later time points after UV irradiation in normal human as well as in XP-E cells, whereas recruitment of ALC1 was absent in dual incision–defective XP-A cells. Fig. S5 shows a significant reduction in CPD repair upon ALC1 depletion or chemical inhibition of PARP1. Table S1 shows the proteins identified in Flag immunoprecipitated material from FLAG-DDB2–expressing MRC5 cells mock treated or irradiated with UV-C. Online supplemental material is available at http://www.jcb.org/cgi/content/full/jcb.201112132/DC1.

References

Aboussekhra, A., M. Biggerstaff, M.K. Shivji, J.A. Vilpo, V. Moncollin, V.N. Podust, M. Protić, U. Hübscher, J.M. Egly, and R.D. Wood. 1995. Mammalian DNA nucleotide excision repair reconstituted with purified protein components. *Cell*. 80:859–868. http://dx.doi.org/10.1016/0092-8674(95)90289-9

Ahel, D., Z. Horejsí, N. Wiechens, S.E. Polo, E. Garcia-Wilson, I. Ahel, H. Flynn, M. Skehel, S.C. West, S.P. Jackson, et al. 2009. Poly(ADP-ribose)-dependent regulation of DNA repair by the chromatin remodeling enzyme ALC1. *Science*. 325:1240–1243. http://dx.doi.org/10.1126/science.1177321

Bryant, H.E., E. Petermann, N. Schultz, A.S. Jemth, O. Loseva, N. Issaeva, F. Johansson, S. Fernandez, P. McGlynn, and T. Helleday. 2009. PARP is activated at stalled forks to mediate Mre11-dependent replication restart and recombination. *EMBO J*. 28:2601–2615. http://dx.doi.org/10.1038/emboj.2009.206

Cleaver, J.E., W.J. Bodell, W.F. Morgan, and B. Zelle. 1983. Differences in the regulation by poly(ADP-ribose) of repair of DNA damage from alkylating agents and ultraviolet light according to cell type. *J. Biol. Chem.* 258:9059–9068.

Cleaver, J.E., E.T. Lam, and I. Revet. 2009. Disorders of nucleotide excision repair: the genetic and molecular basis of heterogeneity. *Nat. Rev. Genet.* 10:756–768. http://dx.doi.org/10.1038/nrg2663

Clement, F.C., U. Camenisch, J. Fei, N. Kaczmarek, N. Mathieu, and H. Naegeli. 2010. Dynamic two-stage mechanism of versatile DNA damage recognition by xeroderma pigmentosum group C protein. *Mutat. Res.* 685:21–28. http://dx.doi.org/10.1016/j.mrfmmm.2009.08.005

Cohen-Armon, M., L. Visochek, D. Rozensal, A. Kalal, I. Geistrikh, R. Klein, S. Bendetz-Nezer, Z. Yao, and R. Seger. 2007. DNA-independent PARP-1 activation by phosphorylated ERK2 increases Elk1 activity: a link to histone acetylation. *Mol. Cell*. 25:297–308. http://dx.doi.org/10.1016/j.molcel.2006.12.012

Datta, A., S. Bagchi, A. Nag, P. Shiyanov, G.R. Adami, T. Yoon, and P. Raychaudhuri. 2001. The p48 subunit of the damaged-DNA binding protein DDB associates with the CBP/p300 family of histone acetyltransferase. *Mutat. Res.* 486:89–97. http://dx.doi.org/10.1016/S0921-8777(01)00082-9

Deng, Z., C. Atanasiu, K. Zhao, R. Marmorstein, J.I. Sbodio, N.W. Chi, and P.M. Lieberman. 2005. Inhibition of Epstein-Barr virus OriP function by tankyrase, a telomere-associated poly-ADP ribose polymerase that binds and modifies EBNA1. *J. Virol.* 79:4640–4650. http://dx.doi.org/10.1128/JVI.79.8.4640-4650.2005

Dinant, C., M. de Jager, J. Essers, W.A. van Cappellen, R. Kanaar, A.B. Houtsmuller, and W. Vermeulen. 2007. Activation of multiple DNA repair pathways by sub-nuclear damage induction methods. *J. Cell Sci.* 120:2731–2740. http://dx.doi.org/10.1242/jcs.004523

Fischer, E.S., A. Scrima, K. Böhm, S. Matsumoto, G.M. Lingaraju, M. Faty, T. Yasuda, S. Cavadini, M. Wakasugi, F. Hanaoka, et al. 2011. The molecular basis of CRL4DDB2/CSA ubiquitin ligase architecture, targeting, and activation. *Cell*. 147:1024–1039. http://dx.doi.org/10.1016/j.cell.2011.10.035

Fitch, M.E., S. Nakajima, A. Yasui, and J.M. Ford. 2003. In vivo recruitment of XPC to UV-induced cyclobutane pyrimidine dimers by the DDB2 gene product. *J. Biol. Chem.* 278:46906–46910. http://dx.doi.org/10.1074/jbc.M307254200

Fousteri, M., W. Vermeulen, A.A. van Zeeland, and L.H. Mullenders. 2006. Cockayne syndrome A and B proteins differentially regulate recruitment of chromatin remodeling and repair factors to stalled RNA polymerase II in vivo. *Mol. Cell*. 23:471–482. http://dx.doi.org/10.1016/j.molcel.2006.06.029

Friedberg, E.C. 2001. How nucleotide excision repair protects against cancer. *Nat. Rev. Cancer*. 1:22–33. http://dx.doi.org/10.1038/35094000

Gagné, J.P., M. Isabelle, K.S. Lo, S. Bourassa, M.J. Hendzel, V.L. Dawson, T.M. Dawson, and G.G. Poirier. 2008. Proteome-wide identification of poly(ADP-ribose) binding proteins and poly(ADP-ribose)-associated protein complexes. *Nucleic Acids Res.* 36:6959–6976. http://dx.doi.org/10.1093/nar/gkn771

Gillet, L.C., and O.D. Schärer. 2006. Molecular mechanisms of mammalian global genome nucleotide excision repair. *Chem. Rev.* 106:253–276. http://dx.doi.org/10.1021/cr040483f

Gottschalk, A.J., G. Timinszky, S.E. Kong, J. Jin, Y. Cai, S.K. Swanson, M.P. Washburn, L. Florens, A.G. Ladurner, J.W. Conaway, and R.C. Conaway. 2009. Poly(ADP-ribosyl)ation directs recruitment and activation of an ATP-dependent chromatin remodeler. *Proc. Natl. Acad. Sci. USA*. 106:13770–13774. http://dx.doi.org/10.1073/pnas.0906920106

Groisman, R., J. Polanowska, I. Kuraoka, J. Sawada, M. Saijo, R. Drapkin, A.F. Kisselev, K. Tanaka, and Y. Nakatani. 2003. The ubiquitin ligase activity in the DDB2 and CSA complexes is differentially regulated by the COP9 signalosome in response to DNA damage. *Cell*. 113:357–367. http://dx.doi.org/10.1016/S0092-8674(03)00316-7

Hassa, P.O., C. Buerki, C. Lombardi, R. Imhof, and M.O. Hottiger. 2003. Transcriptional coactivation of nuclear factor-kappaB-dependent gene expression by p300 is regulated by poly(ADP)-ribose polymerase-1. *J. Biol. Chem.* 278:45145–45153. http://dx.doi.org/10.1074/jbc.M307957200

Houtsmuller, A.B., and W. Vermeulen. 2001. Macromolecular dynamics in living cell nuclei revealed by fluorescence redistribution after photobleaching. *Histochem. Cell Biol.* 115:13–21.

Hwang, B.J., J.M. Ford, P.C. Hanawalt, and G. Chu. 1999. Expression of the p48 xeroderma pigmentosum gene is p53-dependent and is involved in global genomic repair. *Proc. Natl. Acad. Sci. USA*. 96:424–428. http://dx.doi.org/10.1073/pnas.96.2.424

Kapetanaki, M.G., J. Guerrero-Santoro, D.C. Bisi, C.L. Hsieh, V. Rapić-Otrin, and A.S. Levine. 2006. The DDB1-CUL4ADDB2 ubiquitin ligase is deficient in xeroderma pigmentosum group E and targets histone H2A at UV-damaged DNA sites. *Proc. Natl. Acad. Sci. USA*. 103:2588–2593. http://dx.doi.org/10.1073/pnas.0511160103

Kim, J.K., and B.S. Choi. 1995. The solution structure of DNA duplex-decamer containing the (6-4) photoproduct of thymidylyl(3′—>5′)thymidine by NMR and relaxation matrix refinement. *Eur. J. Biochem.* 228:849–854. http://dx.doi.org/10.1111/j.1432-1033.1995.tb20331.x

Krishnakumar, R., and W.L. Kraus. 2010. The PARP side of the nucleus: molecular actions, physiological outcomes, and clinical targets. *Mol. Cell*. 39:8–24. http://dx.doi.org/10.1016/j.molcel.2010.06.017

Luijsterburg, M.S., J. Goedhart, J. Moser, H. Kool, B. Geverts, A.B. Houtsmuller, L.H. Mullenders, W. Vermeulen, and R. van Driel. 2007. Dynamic in vivo interaction of DDB2 E3 ubiquitin ligase with UV-damaged DNA is independent of damage-recognition protein XPC. *J. Cell Sci.* 120:2706–2716. http://dx.doi.org/10.1242/jcs.008367

Luijsterburg, M.S., G. von Bornstaedt, A.M. Gourdin, A.Z. Politi, M.J. Moné, D.O. Warmerdam, J. Goedhart, W. Vermeulen, R. van Driel, and T. Höfer. 2010. Stochastic and reversible assembly of a multiprotein DNA repair complex ensures accurate target site recognition and efficient repair. *J. Cell Biol.* 189:445–463. http://dx.doi.org/10.1083/jcb.200909175

Luijsterburg, M.S., M. Lindh, K. Acs, M.G. Vrouwe, A. Pines, H. van Attikum, L.H. Mullenders, and N.P. Dantuma. 2012. DDB2 promotes chromatin decondensation at UV-induced DNA damage. *J. Cell Biol.* 197:267–281. http://dx.doi.org/10.1083/jcb.201106074

Martin, N., K. Schwamborn, V. Schreiber, A. Werner, C. Guillier, X.D. Zhang, O. Bischof, J.S. Seeler, and A. Dejean. 2009. PARP-1 transcriptional activity is regulated by sumoylation upon heat shock. *EMBO J.* 28:3534–3548. http://dx.doi.org/10.1038/emboj.2009.279

Martinez, E., V.B. Palhan, A. Tjernberg, E.S. Lymar, A.M. Gamper, T.K. Kundu, B.T. Chait, and R.G. Roeder. 2001. Human STAGA complex is a chromatin-acetylating transcription coactivator that interacts with pre-mRNA splicing and DNA damage-binding factors in vivo. *Mol. Cell. Biol.* 21:6782–6795. http://dx.doi.org/10.1128/MCB.21.20.6782-6795.2001

Messner, S., D. Schuermann, M. Altmeyer, I. Kassner, D. Schmidt, P. Schär, S. Müller, and M.O. Hottiger. 2009. Sumoylation of poly(ADP-ribose) polymerase 1 inhibits its acetylation and restrains transcriptional coactivator function. *FASEB J.* 23:3978–3989. http://dx.doi.org/10.1096/fj.09-137695

Messner, S., M. Altmeyer, H. Zhao, A. Pozivil, B. Roschitzki, P. Gehrig, D. Rutishauser, D. Huang, A. Caflisch, and M.O. Hottiger. 2010. PARP1 ADP-ribosylates lysine residues of the core histone tails. *Nucleic Acids Res.* 38:6350–6362. http://dx.doi.org/10.1093/nar/gkq463

Min, J.H., and N.P. Pavletich. 2007. Recognition of DNA damage by the Rad4 nucleotide excision repair protein. *Nature.* 449:570–575. http://dx.doi.org/10.1038/nature06155

Moné, M.J., M. Volker, O. Nikaido, L.H. Mullenders, A.A. van Zeeland, P.J. Verschure, E.M. Manders, and R. van Driel. 2001. Local UV-induced DNA damage in cell nuclei results in local transcription inhibition. *EMBO Rep.* 2:1013–1017. http://dx.doi.org/10.1093/embo-reports/kve224

Moser, J., M. Volker, H. Kool, S. Alekseev, H. Vrieling, A. Yasui, A.A. van Zeeland, and L.H. Mullenders. 2005. The UV-damaged DNA binding protein mediates efficient targeting of the nucleotide excision repair complex to UV-induced photo lesions. *DNA Repair (Amst.).* 4:571–582. http://dx.doi.org/10.1016/j.dnarep.2005.01.001

Moser, J., H. Kool, I. Giakzidis, K. Caldecott, L.H. Mullenders, and M.I. Fousteri. 2007. Sealing of chromosomal DNA nicks during nucleotide excision repair requires XRCC1 and DNA ligase III alpha in a cell-cycle-specific manner. *Mol. Cell.* 27:311–323. http://dx.doi.org/10.1016/j.molcel.2007.06.014

Mu, D., C.H. Park, T. Matsunaga, D.S. Hsu, J.T. Reardon, and A. Sancar. 1995. Reconstitution of human DNA repair excision nuclease in a highly defined system. *J. Biol. Chem.* 270:2415–2418. http://dx.doi.org/10.1074/jbc.270.6.2415

Nishi, R., S. Alekseev, C. Dinant, D. Hoogstraten, A.B. Houtsmuller, J.H. Hoeijmakers, W. Vermeulen, F. Hanaoka, and K. Sugasawa. 2009. UV-DDB-dependent regulation of nucleotide excision repair kinetics in living cells. *DNA Repair (Amst.).* 8:767–776. http://dx.doi.org/10.1016/j.dnarep.2009.02.004

Overmeer, R.M., J. Moser, M. Volker, H. Kool, A.E. Tomkinson, A.A. van Zeeland, L.H. Mullenders, and M. Fousteri. 2011. Replication protein A safeguards genome integrity by controlling NER incision events. *J. Cell Biol.* 192:401–415. http://dx.doi.org/10.1083/jcb.201006011

Palomera-Sanchez, Z., and M. Zurita. 2011. Open, repair and close again: chromatin dynamics and the response to UV-induced DNA damage. *DNA Repair (Amst.).* 10:119–125. http://dx.doi.org/10.1016/j.dnarep.2010.10.010

Pines, A., C. Backendorf, S. Alekseev, J.G. Jansen, F.R. de Gruijl, H. Vrieling, and L.H. Mullenders. 2009. Differential activity of UV-DDB in mouse keratinocytes and fibroblasts: impact on DNA repair and UV-induced skin cancer. *DNA Repair (Amst.).* 8:153–161. http://dx.doi.org/10.1016/j.dnarep.2008.09.011

Rajamohan, S.B., V.B. Pillai, M. Gupta, N.R. Sundaresan, K.G. Birukov, S. Samant, M.O. Hottiger, and M.P. Gupta. 2009. SIRT1 promotes cell survival under stress by deacetylation-dependent deactivation of poly(ADP-ribose) polymerase 1. *Mol. Cell. Biol.* 29:4116–4129. http://dx.doi.org/10.1128/MCB.00121-09

Rapić Otrin, V., I. Kuraoka, T. Nardo, M. McLenigan, A.P. Eker, M. Stefanini, A.S. Levine, and R.D. Wood. 1998. Relationship of the xeroderma pigmentosum group E DNA repair defect to the chromatin and DNA binding proteins UV-DDB and replication protein A. *Mol. Cell. Biol.* 18:3182–3190.

Rapić-Otrin, V., M.P. McLenigan, D.C. Bisi, M. Gonzalez, and A.S. Levine. 2002. Sequential binding of UV DNA damage binding factor and degradation of the p48 subunit as early events after UV irradiation. *Nucleic Acids Res.* 30:2588–2598. http://dx.doi.org/10.1093/nar/30.11.2588

Schultz, N., E. Lopez, N. Saleh-Gohari, and T. Helleday. 2003. Poly(ADP-ribose) polymerase (PARP-1) has a controlling role in homologous recombination. *Nucleic Acids Res.* 31:4959–4964. http://dx.doi.org/10.1093/nar/gkg703

Scrima, A., R. Koníčková, B.K. Czyzewski, Y. Kawasaki, P.D. Jeffrey, R. Groisman, Y. Nakatani, S. Iwai, N.P. Pavletich, and N.H. Thomä. 2008. Structural basis of UV DNA-damage recognition by the DDB1-DDB2

complex. *Cell.* 135:1213–1223. http://dx.doi.org/10.1016/j.cell.2008.10.045

Shiyanov, P., A. Nag, and P. Raychaudhuri. 1999. Cullin 4A associates with the UV-damaged DNA-binding protein DDB. *J. Biol. Chem.* 274:35309–35312. http://dx.doi.org/10.1074/jbc.274.50.35309

Slade, D., M.S. Dunstan, E. Barkauskaite, R. Weston, P. Lafite, N. Dixon, M. Ahel, D. Leys, and I. Ahel. 2011. The structure and catalytic mechanism of a poly(ADP-ribose) glycohydrolase. *Nature.* 477:616–620. http://dx.doi.org/10.1038/nature10404

Sugasawa, K. 2010. Regulation of damage recognition in mammalian global genomic nucleotide excision repair. *Mutat. Res.* 685:29–37. http://dx.doi.org/10.1016/j.mrfmmm.2009.08.004

Sugasawa, K., T. Okamoto, Y. Shimizu, C. Masutani, S. Iwai, and F. Hanaoka. 2001. A multistep damage recognition mechanism for global genomic nucleotide excision repair. *Genes Dev.* 15:507–521. http://dx.doi.org/10.1101/gad.866301

Sugasawa, K., Y. Okuda, M. Saijo, R. Nishi, N. Matsuda, G. Chu, T. Mori, S. Iwai, K. Tanaka, K. Tanaka, and F. Hanaoka. 2005. UV-induced ubiquitylation of XPC protein mediated by UV-DDB-ubiquitin ligase complex. *Cell.* 121:387–400. http://dx.doi.org/10.1016/j.cell.2005.02.035

Tang, J., and G. Chu. 2002. Xeroderma pigmentosum complementation group E and UV-damaged DNA-binding protein. *DNA Repair (Amst.).* 1:601–616. http://dx.doi.org/10.1016/S1568-7864(02)00052-6

Timinszky, G., S. Till, P.O. Hassa, M. Hothorn, G. Kustatscher, B. Nijmeijer, J. Colombelli, M. Altmeyer, E.H. Stelzer, K. Scheffzek, et al. 2009. A macrodomain-containing histone rearranges chromatin upon sensing PARP1 activation. *Nat. Struct. Mol. Biol.* 16:923–929. http://dx.doi.org/10.1038/nsmb.1664

Vodenicharov, M.D., M.M. Ghodgaonkar, S.S. Halappanavar, R.G. Shah, and G.M. Shah. 2005. Mechanism of early biphasic activation of poly(ADP-ribose) polymerase-1 in response to ultraviolet B radiation. *J. Cell Sci.* 118:589–599. http://dx.doi.org/10.1242/jcs.01636

Volker, M., M.J. Moné, P. Karmakar, A. van Hoffen, W. Schul, W. Vermeulen, J.H. Hoeijmakers, R. van Driel, A.A. van Zeeland, and L.H. Mullenders. 2001. Sequential assembly of the nucleotide excision repair factors in vivo. *Mol. Cell.* 8:213–224. http://dx.doi.org/10.1016/S1097-2765(01)00281-7

Wang, H., L. Zhai, J. Xu, H.Y. Joo, S. Jackson, H. Erdjument-Bromage, P. Tempst, Y. Xiong, and Y. Zhang. 2006. Histone H3 and H4 ubiquitylation by the CUL4-DDB-ROC1 ubiquitin ligase facilitates cellular response to DNA damage. *Mol. Cell.* 22:383–394. http://dx.doi.org/10.1016/j.molcel.2006.03.035

Wittschieben, B.O., S. Iwai, and R.D. Wood. 2005. DDB1-DDB2 (xeroderma pigmentosum group E) protein complex recognizes a cyclobutane pyrimidine dimer, mismatches, apurinic/apyrimidinic sites, and compound lesions in DNA. *J. Biol. Chem.* 280:39982–39989. http://dx.doi.org/10.1074/jbc.M507854200

Zotter, A., M.S. Luijsterburg, D.O. Warmerdam, S. Ibrahim, A. Nigg, W.A. van Cappellen, J.H. Hoeijmakers, R. van Driel, W. Vermeulen, and A.B. Houtsmuller. 2006. Recruitment of the nucleotide excision repair endonuclease XPG to sites of UV-induced DNA damage depends on functional TFIIH. *Mol. Cell. Biol.* 26:8868–8879. http://dx.doi.org/10.1128/MCB.00695-06